

## 7. SITE 1079<sup>1</sup>

### Shipboard Scientific Party<sup>2</sup>

#### HOLE 1079A

**Position:** 11°55.7785'S, 13°18.5433'E  
**Start hole:** 1604 hr, 4 September 1997  
**End hole:** 0355 hr, 5 September 1997  
**Time on hole:** 11.85 hr  
**Seafloor (drill pipe measurement from rig floor, mbrf):** 749.2  
**Total depth (drill pipe measurement from rig floor, mbrf):** 870.2  
**Distance between rig floor and sea level (m):** 11.3  
**Water depth (drill pipe measurement from sea level, m):** 737.9  
**Penetration (mbsf):** 121  
**Coring totals:**  
Type: APC  
Number: 14  
Cored: 121 m  
Recovered: 124.61 m (102.98%)  
**Lithology:**  
Unit I: olive-gray silty clay with varying amounts of nannofossils and foraminifers

#### HOLE 1079B

**Position:** 11°55.7676'S, 13°18.5393'E  
**Start hole:** 0355 hr, 5 September 1997  
**End hole:** 1155 hr, 5 September 1997  
**Time on hole:** 8.00 hr  
**Seafloor (drill pipe measurement from rig floor, mbrf):** 749.5  
**Total depth (drill pipe measurement from rig floor, mbrf):** 877.8  
**Distance between rig floor and sea level (m):** 11.3  
**Water depth (drill pipe measurement from sea level, m):** 738.2  
**Penetration (mbsf):** 128.3  
**Coring totals:**  
Type: APC  
Number: 14  
Cored: 128.3 m  
Recovered: 129.7 m (101.1%)  
**Lithology:**  
Unit I: olive-gray silty clay with varying amounts of nannofossils and foraminifers

#### HOLE 1079C

**Position:** 11°55.7969'S, 13°18.5607'E  
**Start hole:** 1155 hr, 5 September 1977  
**End hole:** 2230 hr, 5 September 1997  
**Time on hole:** 10.58 hr  
**Seafloor (drill pipe measurement from rig floor, mbrf):** 749.2  
**Total depth (drill pipe measurement from rig floor, mbrf):** 876  
**Distance between rig floor and sea level (m):** 11.3  
**Water depth (drill pipe measurement from sea level, m):** 737.9  
**Penetration (mbsf):** 126.8  
**Coring totals:**  
Type: APC  
Number: 14  
Cored: 126.8 m  
Recovered: 129.9 m (102.4%)  
**Lithology:**  
Unit I: olive-gray silty clay with varying amounts of nannofossils and foraminifers

**Principal results:** Site 1079 is located outside the Bight of Angola in 1738-m deep water. Situated between the high-productivity regions off the Congo River to the north and off Namibia to the south, the site is part of a transect that will provide information on "pelagic background" sedimentation for the latest Neogene. Sediments from this region indicate lower primary productivity in overlying waters compared with the adjacent upwelling areas. Thus, the influence of the open ocean is more pronounced and will provide a tie-in of coastal ocean history to the record of the pelagic environment. This will allow us to study the cross-correlations of climate-driven ocean dynamics across these two regimes. One of the intriguing aspects of this record is the low opal content associated with high organic matter accumulation. This paradox indicates a strong influence of the quality of subsurface waters, which is set elsewhere in the system, possibly in the Subtropical Convergence Zone. Other topics of importance are the control of variation by precession, reflecting the changing dominance of trade-wind and monsoonal effects.

Three holes were cored with the advanced hydraulic piston corer (APC) at Site 1079 to a maximum depth of 128.3 meters below seafloor (mbsf), which recovered an apparently continuous hemipelagic sedimentary section spanning the last 700 k.y. of the Pleistocene. Hole 1079A was cored with the APC to 121.0 mbsf. Twenty-two cores were taken at Hole 1079B with the APC to a depth of 128.3 mbsf, and Hole 1075C was cored to 126.8 mbsf.

Sediments form one lithostratigraphic unit composed predominantly of uniform olive-gray silty clay with varying amounts of nannofossils and foraminifers. There also are a few discontinuous light olive-gray silt laminae (1–2 mm thickness) present below 80 mbsf. Rare gastropods and frequent shell fragments are disseminated throughout the uppermost 60 mbsf. Whitish gray nodules, 1–2 mm in diameter, are sparse in some of the uppermost cores and become more frequent below 90 mbsf. The calcium carbonate content ranges from 7 to 19 wt%, averaging ~13 wt%.

<sup>1</sup>Wefer, G., Berger, W.H., Richter, C., et al., 1998. *Proc. ODP, Init. Repts.*, 175: College Station, TX (Ocean Drilling Program).

<sup>2</sup>Shipboard Scientific Party is given in the list preceding the Table of Contents.

The silt component is dominated by smectite, kaolinite and/or illite, quartz, the feldspar minerals albite and microcline, and muscovite. The biogenic component is represented by frequent foraminifer fragments and nanofossils. Secondary minerals include dolomite, glauconite, and pyrite. Feldspar, in contrast to quartz, is not supplied by the Congo River; it originates from igneous complexes in southern Africa and therefore probably represents a southern sediment source fed by the Kunene River or eolian dust. Sedimentation rates are high (~400 m/m.y.) in the uppermost 90 mbsf and lower (~50 m/m.y.) between 90 and 120 mbsf.

Detailed comparisons between the magnetic susceptibility record generated on the multisensor track (MST) and high-resolution color reflectance measured with the Minolta spectrophotometer demonstrated complete recovery of the sedimentary sequence down to 132 meters composite depth (mcd).

Preservation of calcareous nanofossil specimens is good to very good. The overall abundance ranges from very abundant to abundant throughout the entire section. Reworked specimens (Neogene) are rare to common between 90 and 120 mbsf. Based on the oldest identified datum, the bottom age of Hole 1079A is estimated at  $0.7 \pm 0.05$  Ma. The benthic foraminifers are well preserved and abundant at Site 1079; however, the diversity is relatively low and dominated by *Bolivina* species. Planktonic foraminifers are common in the upper 50 mbsf, but abundance levels fall drastically below 60 mbsf. Diatoms, silicoflagellates, and radiolarians are absent throughout the entire section.

Magnetic inclinations and declinations after alternating-field (AF) demagnetization at 20 mT indicate that only the Brunhes (C1n) normal polarity Chron is recorded. Short reversal events in the Brunhes Chron were not found, despite the high sedimentation rates.

Sediments average 3.0 wt% total organic carbon (TOC), which is high for ocean margin areas and reflects a history of elevated primary production in this area. Interstitial water chemistry studies document a sequence of diagenetic processes in the upper 50 mbsf that are caused largely by the degradation of organic matter and carbonate dissolution-reprecipitation reactions. Among these are moderately high levels of methane and carbon dioxide generated by in situ microbial activity. Increases in interstitial water sulfate, chloride, and salinity from 70 mbsf to the bottom of Hole 1079A at 120 mbsf may reflect the influence of evaporite dissolution and brine formation. Profiles of salinity, dissolved chloride, and methane do not indicate the presence of gas hydrate in Site 1079 sediments.

Physical sediment properties were determined both by high-resolution MST core logging and index properties measurements. Magnetic susceptibility and gamma-ray attenuation porosity evaluator (GRAPE) signals reveal pronounced cyclicities, which were used for high-quality stratigraphic correlation in conjunction with digital color data.

Site 1079 was drilled as a companion to Site 1078 to make an east-west transect in the Eastern Angola Basin. High regional productivity and a strong influx of terrigenous clays and silts from a rapidly rising shore (with cliffs and deep, narrow canyons near Lobito) provide an expanded record of the late Quaternary. High productivity is greatly favored by the supply of nutrients from subsurface waters, probably involving the Angola Dome. Changes in productivity should record the intensity of domal and coastal upwelling and, possibly, the movement of the Angola-Benguela Front. Variations in the supply of marine water or terrigenous matter will track climate changes in the drainage basins supplying the sediment, as well as the rates of uplift along the Angolan coast. Such uplift could be caused by salt tectonics below the shelf, stimulated by increasing amplitudes of sea-level change. If so, terrigenous influx should have greatly increased during the last 1 m.y.

## BACKGROUND AND OBJECTIVES

For a discussion of the background and objectives for Site 1079, see "Background and Objectives" section, "Site 1078" chapter (this volume).

## OPERATIONS

### Hole 1079A (Proposed Site MAB-2)

The vessel proceeded in dynamic positioning (DP) mode to the Global Positioning System coordinates of Site 1079, where a beacon was deployed at 1604 hr on 4 September. A second beacon was dropped at 1650 hr as a precautionary measure because of erratic acoustics initially attributed to a distorted beacon signal. It was later determined that fishing boats in the area were transmitting signals that temporally affected the DP system and the precision depth recorder. Hole 1079A was spudded at 2007 hr on 4 September. The sea-floor depth was established at 737.9 meters below sea level (mbsl) by drill-pipe measurement (DPM). APC Cores 175-1079A-1H through 14H were taken from 0 to 121.0 mbsf (Table 1; also see the expanded core summary table on CD-ROM, back pocket, this volume), with 121.0 m cored and 124.6 m recovered (103.0%). Cores were oriented starting with Core 4H. No Adara heat-flow measurements were taken at this site. The drill string was pulled out of the hole with the top

Table 1. Coring summary for Site 1079.

Core	Date (Sept 1997)	Time (UTC)	Interval (mbsf)	Length cored (m)	Length recovered (m)	Recovery (%)
<b>175-1079A-</b>						
1H	4	2015	0.0-5.3	5.3	5.34	100.8
2H	4	2045	5.3-14.8	9.5	9.91	104.3
3H	4	2110	14.8-24.3	9.5	10.03	105.6
4H	4	2135	24.3-33.8	9.5	9.79	103.1
5H	4	2205	33.8-43.3	9.5	9.82	103.4
6H	4	2235	43.3-52.8	9.5	9.94	104.6
7H	4	2305	52.8-62.3	9.5	10.09	106.2
8H	4	2340	62.3-71.8	9.5	10.23	107.7
9H	5	0010	71.8-81.3	9.5	9.53	100.3
10H	5	0055	81.3-90.8	9.5	10.89	114.6
11H	5	0125	90.8-100.3	9.5	8.26	86.9
12H	5	0150	100.3-108.4	8.1	8.13	100.4
13H	5	0225	108.4-117.2	8.8	8.78	99.8
14H	5	0305	117.2-121.0	3.8	3.87	101.8
Coring totals:				121.0	124.61	103.0
<b>175-1079B-</b>						
1H	5	0440	0.0-7.0	7.0	7.06	100.9
2H	5	0500	7.0-16.5	9.5	9.68	101.9
3H	5	0540	16.5-26.0	9.5	9.59	100.9
4H	5	0610	26.0-35.5	9.5	9.89	104.1
5H	5	0640	35.5-45.0	9.5	9.68	101.9
6H	5	0705	45.0-54.5	9.5	9.71	102.2
7H	5	0730	54.5-64.0	9.5	9.32	98.1
8H	5	0750	64.0-73.5	9.5	10.08	106.1
9H	5	0820	73.5-82.5	9.0	9.09	101.0
10H	5	0845	82.5-92.0	9.5	9.27	97.6
11H	5	0915	92.0-100.0	8.0	8.15	101.9
12H	5	0945	100.0-109.5	9.5	9.63	101.4
13H	5	1030	109.5-119.0	9.5	9.27	97.6
14H	5	1105	119.0-128.3	9.3	9.28	99.8
Coring totals:				128.3	129.70	101.1
<b>175-1079C-</b>						
1H	5	1230	0.0-3.3	3.3	3.31	100.3
2H	5	1255	3.3-12.8	9.5	9.57	100.7
3H	5	1315	12.8-22.3	9.5	9.96	104.8
4H	5	1345	22.3-31.8	9.5	9.82	103.4
5H	5	1410	31.8-41.3	9.5	9.85	103.7
6H	5	1440	41.3-50.8	9.5	9.59	100.9
7H	5	1510	50.8-60.3	9.5	9.22	97.1
8H	5	1535	60.3-69.8	9.5	9.02	94.9
9H	5	1605	69.8-79.3	9.5	10.96	115.4
10H	5	1635	79.3-88.8	9.5	10.09	106.2
11H	5	1710	88.8-98.3	9.5	9.19	96.7
12H	5	1740	98.3-107.8	9.5	10.34	108.8
13H	5	1830	107.8-117.3	9.5	9.68	101.9
14H	5	1920	117.3-126.8	9.5	9.30	97.9
Coring totals:				126.8	129.90	102.4

Notes: UTC = Universal Time Coordinated. An expanded version of this coring summary table that includes lengths and depths of sections and comments on sampling is included on CD-ROM (back pocket, this volume).

drive, and the bit cleared the sea floor at 0355 hr on 5 September, thereby ending Hole 1079A.

### Hole 1079B

The vessel was offset 30 m to the south, and Hole 1079B was spudded with the APC at 0430 hr on 5 September. The seafloor depth was established at 738.2 mbsl by DPM. APC Cores 175-1079B-1H through 14H were taken from 0 to 128.3 mbsf (Table 1), with 128.3 m cored and 129.7 m recovered (101.1% recovery). Cores were oriented starting with Core 3H. The drill string was pulled out of the hole and cleared the seafloor at 1155 hr on 5 September, ending Hole 1079B.

### Hole 1079C

The vessel was offset 30 m to the south, and Hole 1079C was spudded with the APC at 1225 hr on 5 September. The seafloor depth was established at 737.9 mbsl by DPM. APC Cores 175-1079C-1H through 14H were taken from 0 to 126.8 mbsf (Table 1), with 126.8 m cored and 129.9 m recovered (102.4% recovery). Cores were oriented starting with Core 4H. The drill string was pulled out of the hole and cleared the seafloor at 2035 hr on 5 September, ending operations at Site 1079.

## SITE GEOPHYSICS

For a discussion of site geophysics at Site 1079, see "Site Geophysics" section, "Site 1078" chapter (this volume).

## LITHOSTRATIGRAPHY

### Introduction

Three holes were drilled with the APC at Site 1079, with a maximum penetration of 129.9 mbsf. The last sections of Holes 1079A and 1079B, as well as several sections from Hole 1079C, possessed flow-in structures, such as pseudo-bedding, parallel to the core liner and 1- to 2-cm-wide tubular structures penetrating the entire section (see barrel sheets, Section 4, this volume). Additional core disturbances caused by gas expansion are common at Site 1079.

### Description of Lithostratigraphic Unit

The lithostratigraphic description for the sedimentary sequence from Site 1079 is based on data from the following sources: (1) visual core description, (2) smear-slide examination, (3) color reflectance measurements, (4) bulk calcium carbonate measurements, and (5) X-ray diffraction (XRD) measurements.

Sediments from Site 1079 form one lithostratigraphic unit composed predominantly of uniform olive-gray (5Y 4/2) silty clay with varying amounts of nannofossils and foraminifers (see Fig. 1). There are also a few discontinuous light olive-gray silt laminae (1–2 mm in thickness), which are present below 80 mbsf at all three holes. Rare gastropod shells and shell fragments in frequent abundance are disseminated throughout the uppermost seven cores of all three holes. Bioturbation is evident from numerous burrows filled with lighter colored clay. Whitish gray nodules, 1–2 mm in diameter, are present, but rare, in some of the uppermost cores. They become more frequent below 90 mbsf. Calcium carbonate content of the sediment ranges from 7 to 19 wt%, averaging about 13 wt%.

A 60-cm-thick turbidite is present in interval 175-1079C-10H-5, 35–110 cm. The base of the interval (Section 175-1079-10H-5) at 110 cm is a scoured contact (see Fig. 2). The lower part of the turbid-

ite consists of coarse silt, which grades upward into clay. Above the turbidite sequence is a thinly laminated package of alternating layers of dark olive-gray, dark gray clay, and light olive-gray silt. Bioturbated silty clay intervals at the top and bottom of the laminated package indicate that the low oxygen content of bottom waters may have been important in preserving laminae.

### Synthesis of Smear-Slide Analyses

Smear-slide analyses indicate that silty clay is the dominant lithology at Site 1079. The silt component is dominated by subangular and angular mono- and polycrystalline quartz grains with subordinate amounts of detrital angular feldspar grains. Muscovite and biotite are present in trace amounts. The biogenic component is represented by frequent foraminifer fragments and nannofossils. Secondary minerals include dolomite, glauconite, and pyrite. The thin, 1- to 2-mm-thick, light olive-gray silty layers contain angular quartz and feldspar grains that are coarser than those in the clay layers.

### X-ray Diffraction Analysis

XRD analysis of sediments from Hole 1079A reveals that the clastic fraction is dominated by smectite, kaolinite/illite, quartz, the feldspar minerals albite and microcline, and muscovite. Pyrite was identified as an accessory mineral in all samples. Other accessory phases could not be clearly identified using XRD. The smectites are generally poorly crystallized. Quartz and feldspar show comparable downcore variations, which are probably caused by grain-size variations (see Fig. 3). In contrast to quartz, feldspar is not supplied by the Congo River (van der Gaast and Jansen, 1984). Feldspar originates from igneous complexes in southern Africa and therefore probably represents a southern sediment source fed by the Kunene River or by eolian dust. Consequently, the feldspar/quartz ratio may indicate the contribution of sediment supplied from the south.

### Spectrophotometry

Color data were measured every 2 cm for Hole 1079A. Holes 1079B and 1079C were measured at 4-cm intervals. The reflectance data range between 30% and 45% throughout the column recovered from Site 1079. The red/blue (650 nm/450 nm) ratio (Fig. 4) and total reflectance (Fig. 5) data were smoothed over nine points for Hole 1079A and over five points for Holes 1079B and 1079C to remove smaller scale variability. Core disturbance makes correlation between holes difficult. After an initial high extending over 10 m, the red/blue ratio shows a low variability downcore. Comparison between the total reflectance and the red/blue ratio with calcium carbonate content and organic carbon shows no correlation (Figs. 6, 7).

## BIOSTRATIGRAPHY AND SEDIMENTATION RATES

Sediments recovered from Site 1079 represent a relatively continuous hemipelagic section spanning the last ~700 k.y. of the Pleistocene. The calcareous micropaleontological study was carried out on core-catcher samples from Hole 1079A. Additional samples from within the cores were examined for calcareous nannofossil biostratigraphy. Diatoms, silicoflagellates, and radiolarians are absent.

### Calcareous Nannofossils

Calcareous nannofossils were studied in core-catcher samples from Hole 1079A. Additional samples from within the cores were examined close to datum events to improve the stratigraphic resolution. Preservation of nannofossil specimens is good to very good. The

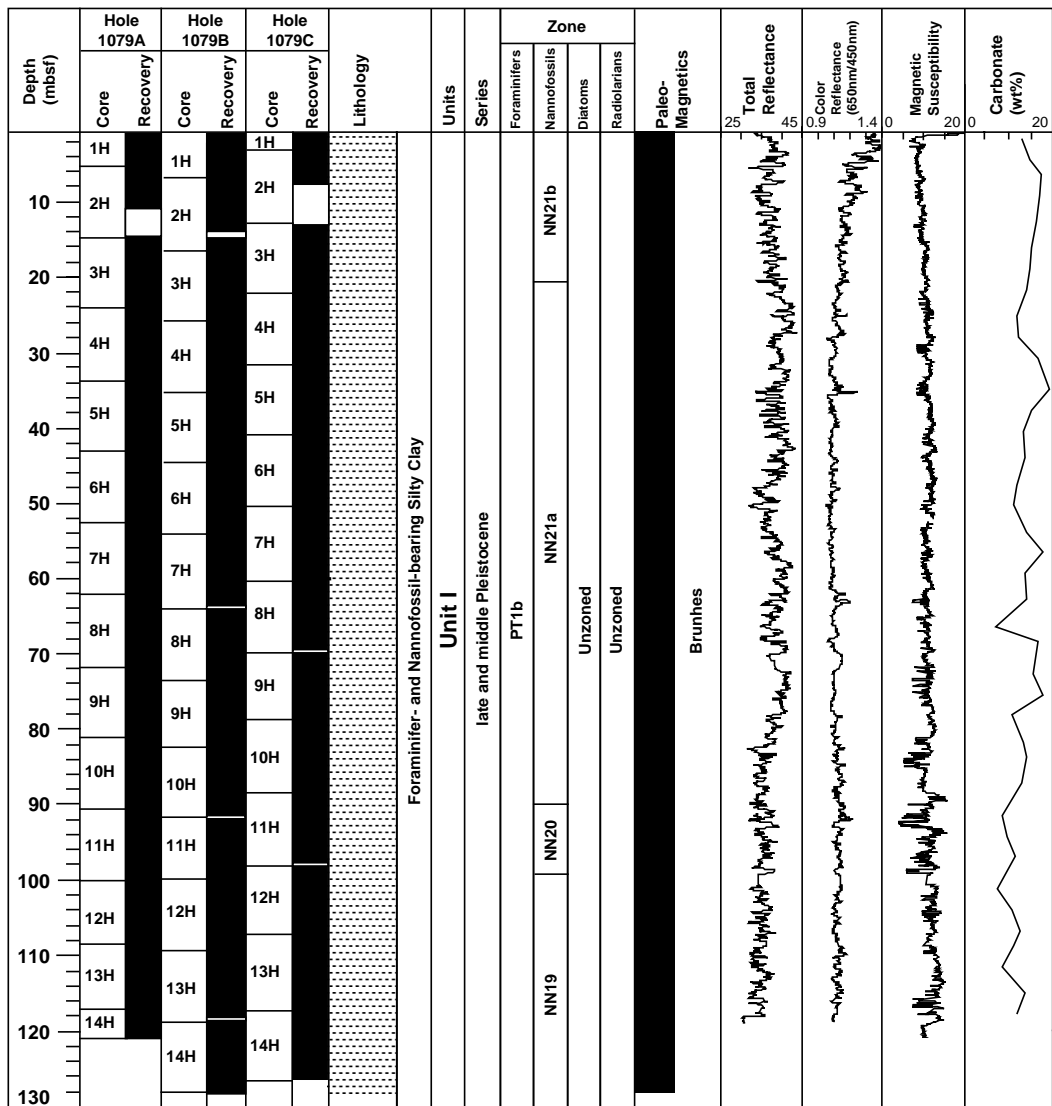


Figure 1. Composite stratigraphic section for Site 1079 showing core recovery in all holes, a simplified summary of lithology, biostratigraphic zonations, total reflectance (400–700 nm), color reflectance (650 nm/450 nm), magnetic susceptibility, and calcium carbonate content.

overall abundance ranges from very abundant to abundant throughout the entire section. Reworked specimens (Neogene) are rare to common in Cores 175-1079A-10H through 13H.

The nannofossil-based biostratigraphy (Table 2; Fig. 8) indicates that Site 1079 terminated within the upper part of Zone NN19. Based on the oldest identified datum (last occurrence [LO] of *Small Gephyrocapsa acme* sensu Weaver [1993]) and paleomagnetic evidence (see “Paleomagnetism” section, this chapter), the bottom age of Hole 1079A is estimated at  $0.7 \pm 0.05$  Ma. Within the sampling resolution, the sedimentation appears continuous throughout the entire section. Sedimentation rates show a step-like pattern, with a maximum of 40 cm/k.y. within Zone NN21a (i.e., from the top of isotope Stage 5 [~0.09 Ma] to the middle part of isotope Stage 8 [0.26 Ma]). This maximum value agrees with the one recorded within the same stratigraphic interval (60 cm/k.y.) in the nearby shallower Site 1078.

**Zone NN21b**

The first occurrence of the *Emiliania huxleyi* acme, which defines the Zone NN21b/NN21a boundary, was recognized between Sam-

ples 175-1079A-3H-3, 130 cm, and 3H-CC. This datum event is near-synchronous with a planktonic foraminiferal datum event (LO of *Globorotalia tumida flexuosa*, 0.07 Ma) found within Core 175-1079A-3H. Sedimentation rate within this top interval is >23 cm/k.y.

**Zone NN21a**

This stratigraphic interval spans most of the section at Site 1079. The LO of the *Gephyrocapsa caribbeanica* acme (Weaver, 1993), which marks the Zone NN21a/NN20 boundary, was identified between Samples 175-1079A-10H-5, 80 cm, and 10H-CC.

**Zone NN20**

As documented at Sites 1077, 1076, and 1075, this interval spanning 0.2 m.y. from mid-isotope Stage 8 to mid-isotope Stage 12 is constrained within a narrow depth range (~10 m). The Zone NN21a/NN20 boundary was identified within the lower part of Core 175-1079A-11H.

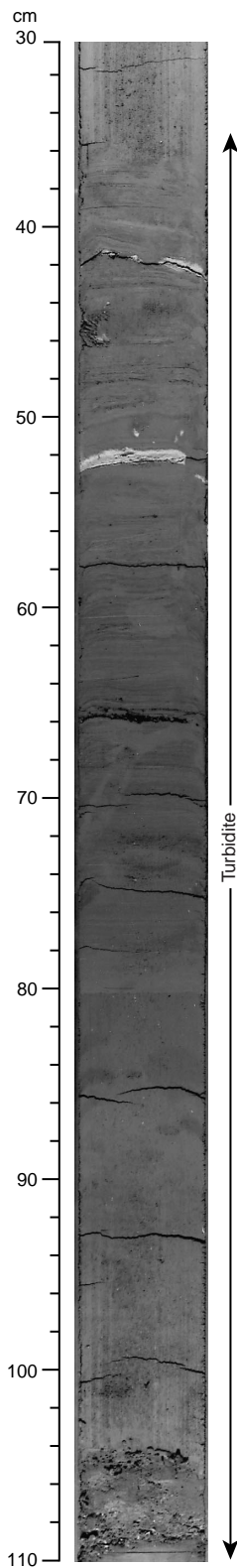


Figure 2. Photograph of turbidite located in interval 175-1079C-10H-5, 35–110 cm. The scoured base at 100 cm grades from coarse silt upward to clay and is overlain by a thinly laminated package of alternating layers of dark olive-gray, dark gray clay, and light olive-gray clay. Bioturbation occurs above and below the package.

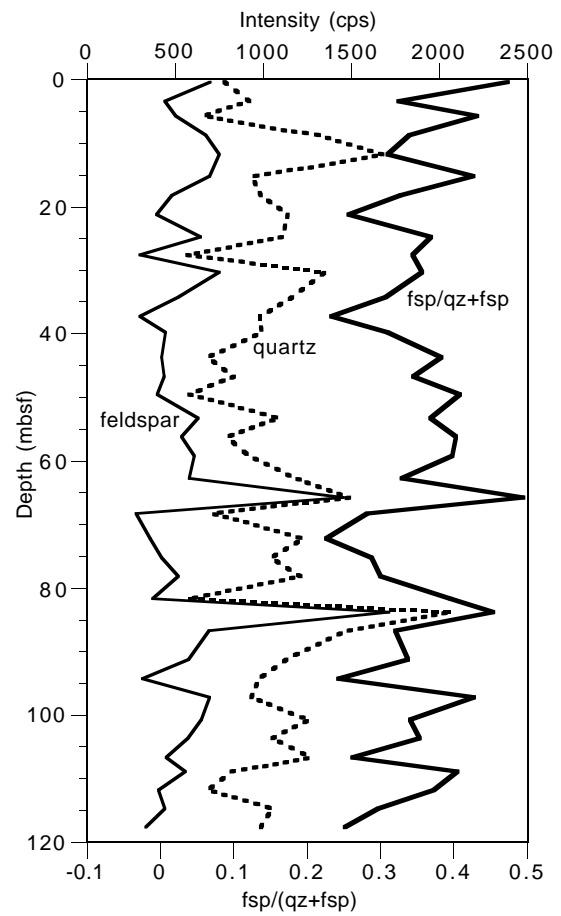


Figure 3. Stratigraphic variation in the quartz and feldspar peak intensity (in counts per second [cps]) derived from the XRD patterns.

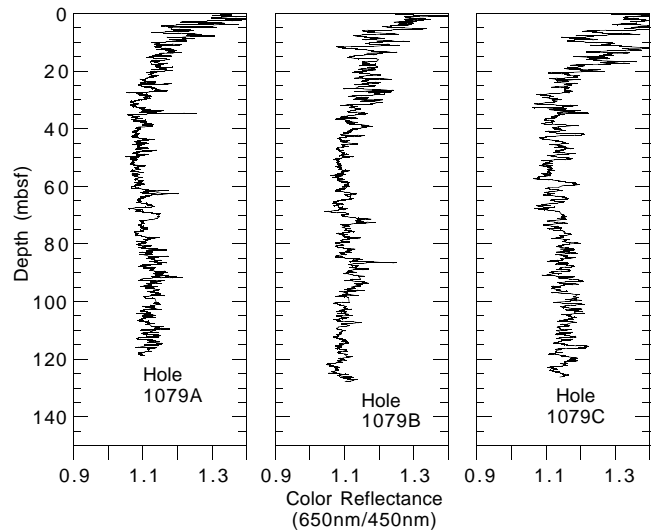


Figure 4. Stratigraphic variation in the ratio of the red (650 nm) to blue (450 nm) wavelengths at Holes 1079A, 1079B, and 1079C. A five-point smoothing procedure was applied to the data set.

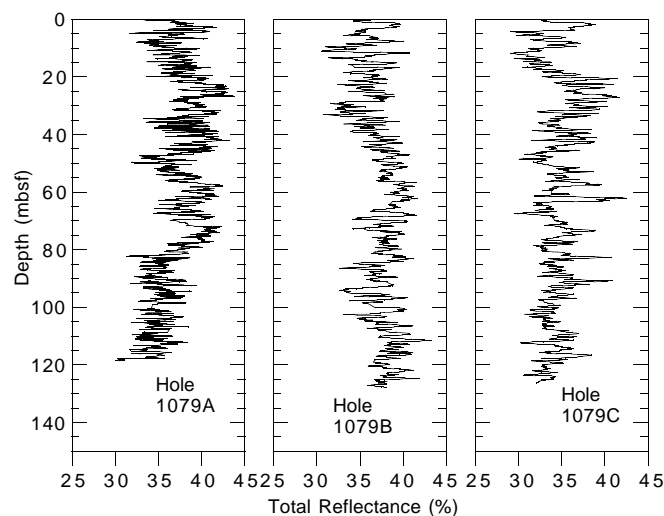


Figure 5. Stratigraphic variation in the total reflectance of visible light (400–700 nm) at Holes 1079A, 1079B, and 1079C. A nine-point smoothing procedure was applied to the data set.

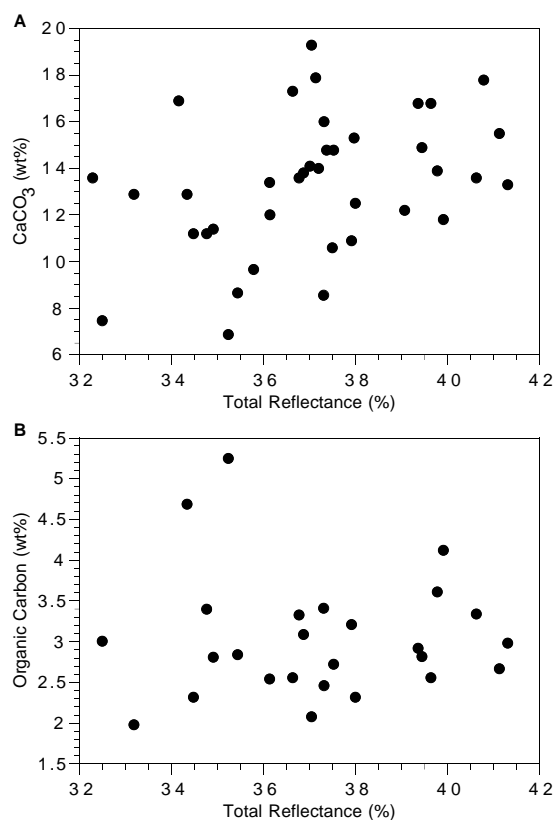


Figure 6. Relationship between the total reflectance spectral ratio and the concentrations of (A) calcium carbonate and (B) organic carbon at Hole 1079A.

**Zone NN19**

The LO of the Small *Gephyrocapsa* acme (Weaver, 1993), the only identified datum event within this bottom interval, was found between Samples 175-1079A-12H-CC and 13H-2, 140 cm.

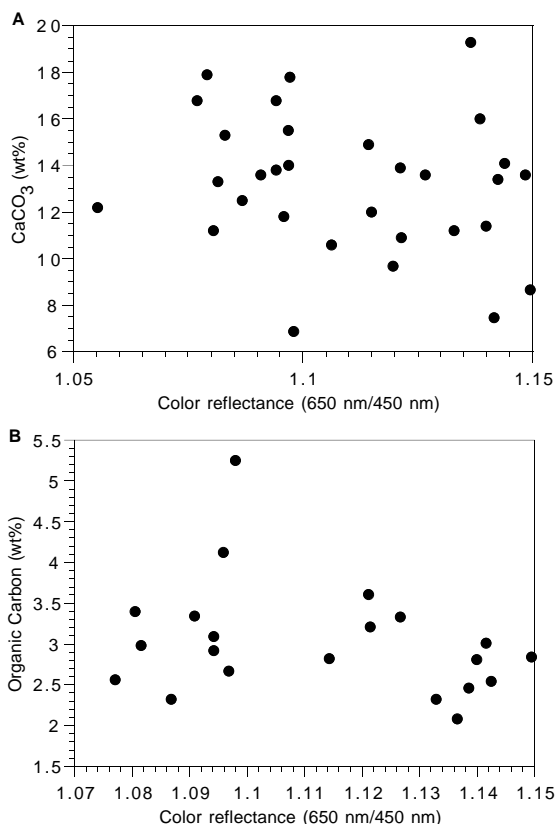


Figure 7. Relationship between the red/blue wavelength spectral ratio and the concentrations of (A) calcium carbonate and (B) organic carbon at Hole 1079A.

**Planktonic Foraminifers**

Planktonic foraminifers are common in the upper six cores, but abundance levels fall to few in Cores 175-1079A-7H-CC, 9H-CC, and 10H-CC and to trace levels in Sample 14H-CC. The low abundance in Sample 175-1079A-14H-CC is attributed to dissolution, but the other intervals may have lower abundances caused by dilution from increased terrigenous input.

Near this site, the cold surface Benguela Current and the warm, southward-flowing surface Angola Current converge, and downcore variations should reflect the change in the position of the Angola-Benguela Front. The uppermost assemblage at Hole 1079A (5.3 mbsf) is dominated by high abundances of *Orbulina universa*, *Globigerinoides sacculifer*, *Globigerinella siphonifera*, and *Neoglobobulimina pachyderma* (dextral) (Table 3). Other species that are present but not abundant are *Globigerinoides ruber* (pink and white), *Globigerina bulloides*, *Globorotalia crassaformis*, *Neoglobobulimina dutertrei*, *Neoglobobulimina pachyderma* (sinistral), *Globorotalia inflata*, and *Pulleniatina obliquiloculata* (Table 3).

*Globorotalia tumida flexuosa* is present in Samples 175-1079A-3H-CC, 4H-CC, and 12H-CC and constrains the age to no younger than 0.07 Ma. This is in agreement with the calcareous nannofossil biostratigraphy.

The change in fauna downcore is similar to the change at Site 1078. In Sample 175-1079A-8H-CC (72.5 mbsf) and below, *N. pachyderma* is abundant, but above this level, it is only present in the uppermost assemblage (5.3 mbsf) at high abundances (Table 3). Samples 175-1079A-2H-CC through 7H-CC are dominated by *G. ruber*, *G. sacculifer*, and *G. bulloides*, indicating a change to warmer surface-water conditions (Table 3). This change in fauna from abundant *N. pachyderma* to abundant *G. ruber* apparently occurs at the

**Table 2. Calcareous nannofossil datums at Hole 1079A.**

Event	Age (Ma)	Zone (base)		Core, section, interval (cm)		Depth (mbsf)		
		A	B	Top	Bottom	Top	Bottom	Mean
FO <i>Emiliana huxleyi</i> acme	0.09	NN21b		175-1079A-3H-3, 130	175-1079A-3H-5, 130	19.10	22.10	20.60
FO <i>Emiliana huxleyi</i>	0.26	NN21a	CN15	10H-5, 80	10H-CC	87.09	92.14	89.62
LO <i>Gephyrocapsa caribbeanica</i> acme	0.26	NN21a	CN15	10H-5, 80	10H-CC	87.09	92.14	89.62
LO <i>Pseudoemiliana lacunosa</i>	0.46	NN20	CN14b	11H-5, 70	11H-CC	97.40	99.01	98.21
LO Small <i>Gephyrocapsa</i> acme (Weaver, 1993)	0.6*			12H-CC	13H-2, 140	108.38	111.30	109.84

Notes: FO = first occurrence and LO = last occurrence. \* = lower isotope Stage 15 (Weaver, 1993); age interpolated from Imbrie et al. (1984). Zonal codes are those of (A) Martini (1971) and (B) Okada and Bukry (1980).

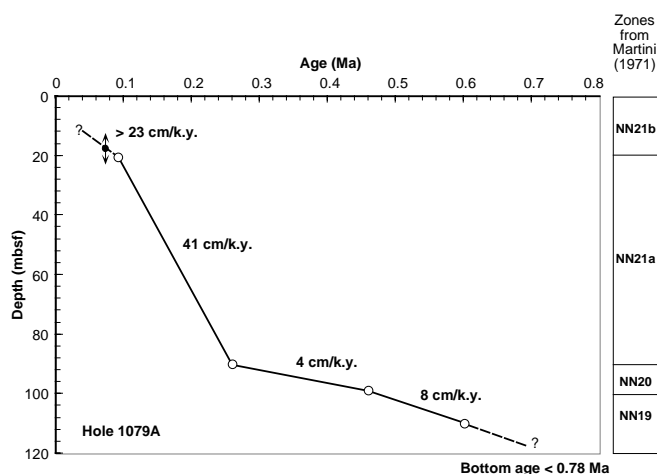


Figure 8. Age-depth plot and sedimentation rates estimated from calcareous nannofossil datums at Hole 1079A. The double arrow points to the depth range of the planktonic foraminiferal datum event (LO of *Globorotalia tumida flexuosa*).

same stratigraphic level as at Site 1078, near 0.25 Ma. *G. crassaformis* is abundant in Samples 175-1079A-6H-CC and 12H-CC. The species is associated with the Equatorial Undercurrent (Bé and Tolderrlund, 1971) and may represent greater southern penetration of this current in the past.

### Benthic Foraminifers

The benthic foraminifers are well preserved and abundant in all core catchers from Hole 1079A, except for Sample 175-1079A-14H-CC, which is barren. The diversity is relatively low, as at the nearby, slightly shallower Site 1078. Most of the samples are dominated by *Bolivina* sp. 1 and *Bolivina* sp. 2. Additional contribution comes from *Bulimina exilis*, *Cassidulina leavigata*, and the *Praeglobulimina/Globobulimina* group (Table 4; Fig. 9). Variations in the relative abundance occur but do not show any significant changes that can be attributed to major environmental changes. *Hyalinea balthica* shows a single large peak in Sample 175-1079A-3H-CC (27%), and *Uvigerina auberiana* peaks in Sample 175-1079A-13H-CC (32%). The absence of benthic foraminifers in Sample 14H-CC (121.02 mbsf) may be of local character because samples above and below this depth at Hole 1079B (Sample 175-1079B-13H-CC [118.72 mbsf] and Sample 14H-CC [128.23 mbsf]) have abundant benthic foraminifers.

As at Site 1078, the dominance of *Bolivina* sp. 1 and *Bolivina* sp. 2 and the overall low faunal diversity suggest low oxygen concentrations at the seafloor (see "Biostratigraphy and Sedimentation Rates" section, "Site 1078" chapter, this volume). The average contribution of *Bolivina* sp. 1 and *Bolivina* sp. 2, is, however, somewhat lower at

**Table 3. Dominant and abundant planktonic foraminiferal species at Hole 1079A.**

Core, section, interval	Depth (mbsf)	Abundance											
		<i>Globigerinoides ruber</i> (pink)	<i>Globigerinoides ruber</i>	<i>Orbulina universa</i>	<i>Globigerinoides sacculifer</i>	<i>Globigerina bulloides</i>	<i>Globigerinella siphonifera</i>	<i>Globorotalia inflata</i>	<i>Neogloboquadrina daterrei</i>	<i>Neogloboquadrina pachyderma</i> (dextral)	<i>Neogloboquadrina pachyderma</i> (sinistral)	<i>Globorotalia crassaformis</i>	<i>Globorotalia tumida flexuosa</i>
175-1079A-1H-CC	5.3												
2H-CC	15.2	A	D										
3H-CC	24.8		A	A	A								
4H-CC	34.0		A	D	A								P
5H-CC	43.6		A	D	D	A							P
6H-CC	53.2		A	A			A	A					A
7H-CC	62.8	F	A	D									
8H-CC	72.5		A	D		A							
9H-CC	81.3	F	A	A						A			
10H-CC	92.1	F	A	D						A	A		
11H-CC	99.0		A	D				A		A	A		
12H-CC	108.4		A							A	A	A	P
13H-CC	117.1		A	A							D		
14H-CC	121.0	T											

Notes: D = dominant (>30%) and A = abundant (10%–30%). Intervals of low abundance of total assemblage (T = trace and F = few) are shown and are attributed to dissolution. P = intervals where *G. tumida flexuosa* is present.

Site 1079 (~60%) than at Site 1078 (~85%), which may reflect less severe oxygen depletion at the seafloor at the former.

### Diatoms and Radiolarians

Core-catcher samples from Holes 1079A, 1078B, and 1079C were analyzed for their diatom and radiolarian contents. Samples were prepared as smear slides (for diatoms) and acid-cleaned (for both microfossil groups). The treated samples were washed with distilled water and sieved through 20- $\mu$ m, 38- $\mu$ m, or 63- $\mu$ m sieves. Diatoms and radiolarians are absent in almost all core-catcher samples. Trace amounts are found in Samples 175-1079A-1H-CC, 4H-CC, and 6H-CC.

### PALEOMAGNETISM

The investigation of magnetic properties at Site 1079 included the measurement of bulk susceptibility of whole-core sections and the natural remanent magnetization (NRM) of archive-half sections. The Tensor tool was used to orient Cores 175-1079A-4H through 14H,



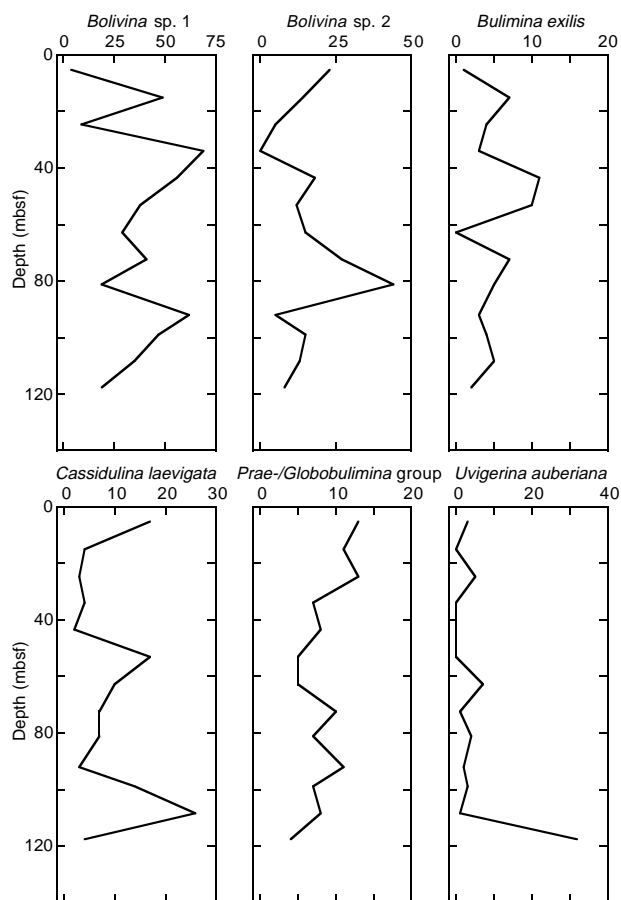


Figure 9. Relative abundances (in percentages) of selected benthic foraminiferal species at Hole 1079A.

175-1079B-3H through 14H, and 175-1079C-4H through 14H (Table 5).

### Natural Remanent Magnetization and Magnetic Susceptibility

Magnetic susceptibility measurements were made on whole cores from all three holes as part of the MST analysis (see “Physical Properties” section, this chapter). Magnetic susceptibility ranges from  $\sim 5$  to  $15 \times 10^{-5}$  (SI volume units; Fig. 10) and is relatively constant with depth, except for a low between  $\sim 3$  and 15 mbsf.

Measurements of NRM were made on all archive-half core sections from Holes 1079A, 1079B, and 1079C. Sections from Hole 1079A were demagnetized by AF at 10 and 20 mT; sections from Holes 1079B and 1079C were demagnetized by AF at 20 mT only.

A primary magnetic component was preserved in sediments from all three holes. The intensity of NRM after 20-mT demagnetization from the three holes is similar in magnitude and trend, ranging generally from  $\sim 10^{-4}$  to  $\sim 10^{-2}$  A/m (Fig. 11, left panel). Fluctuations of about an order of magnitude are superimposed on an overall decreasing trend with depth. The large intensity variation contrasts with the relatively constant magnetic susceptibility.

The variation pattern of remanent intensity at Site 1079 closely resembles that at Site 1078 (see “Paleomagnetism” section, “Site 1078” chapter, this volume). Between the two horizons of nannofossil events (at 0.09 and 0.26 Ma; see “Biostratigraphy and Sedimentation Rates” section, this chapter, and “Site 1078” chapter, this volume),

Table 5. Tensor tool-orientation data for cores from Holes 1079A, 1079B, and 1079C.

Core	MTF (°)	Inclination angle
175-1079A-		
4H	332	0.85
5H	63	1.16
6H	99	1.13
7H	357	0.95
8H	305	0.86
9H	322	0.78
10H	100	0.46
11H	186	0.49
12H	29	0.81
13H	248	0.66
14H	90	0.50
175-1079B-		
3H	52	0.41
4H	58	0.47
5H	156	0.55
6H	359	0.38
7H	48	0.23
8H	323	0.24
9H	352	0.25
10H	222	0.39
11H	140	0.29
12H	222	0.32
13H	229	0.26
14H	332	0.26
175-1079C-		
4H	287	1.16
5H	294	1.03
6H	164	1.04
7H	235	0.96
8H	336	1.12
9H	224	1.18
10H	353	1.26
11H	129	1.36
12H	53	1.42
13H	321	1.34
14H	352	1.34

Notes: The orientation parameter (MTF) is the angle in degrees between magnetic north and the double line marked on the center of the working half of the core. The local declination anomaly is  $9^\circ$ W.

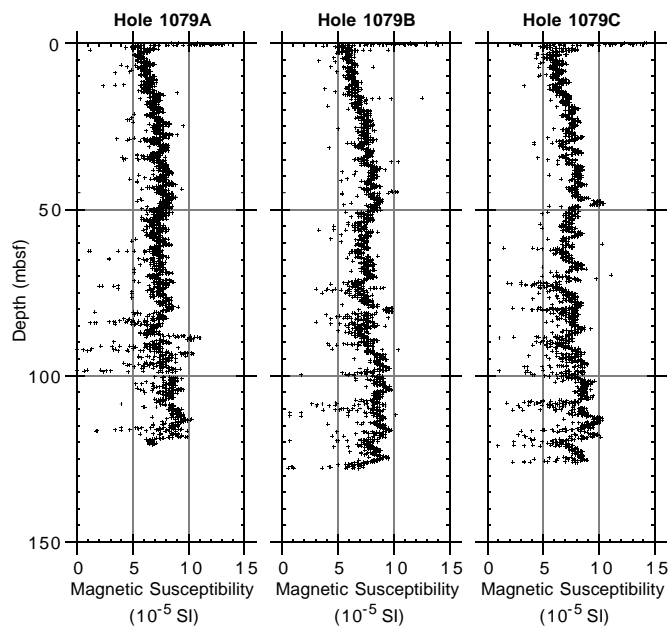


Figure 10. Magnetic susceptibilities from MST data (volume corrected) for Holes 1079A, 1079B, and 1079C.

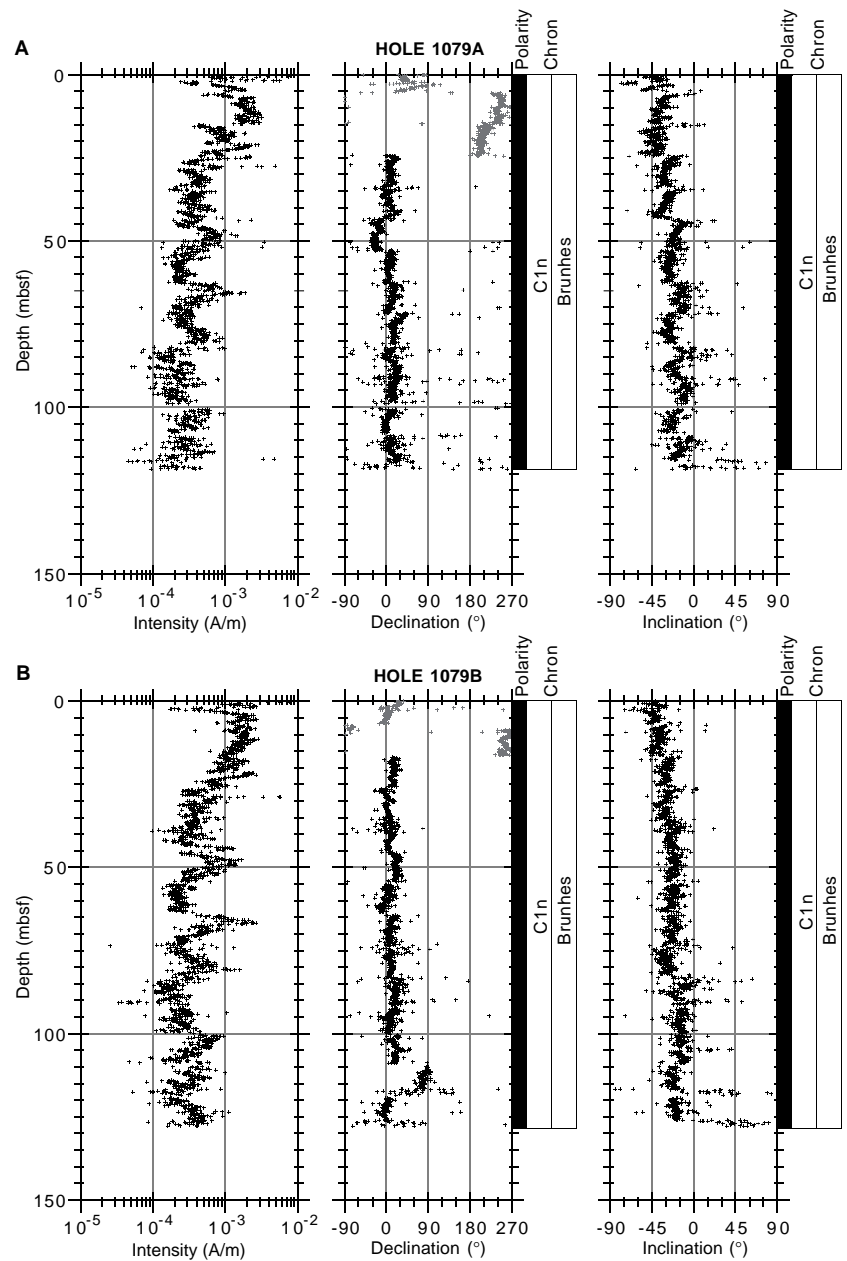


Figure 11. NRM intensity, declination, inclination, and magnetostratigraphic interpretation after 20-mT demagnetization. Black symbols = Tensor corrected; gray symbols = uncorrected. Polarity shading: black = normal. **A.** Hole 1079A. **B.** Hole 1079B. (Continued on next page.)

sediments at Sites 1078 and 1079 can be correlated using the remanent intensity (Fig. 12). The intensity of NRM can be controlled by the strength of the geomagnetic field, the concentration of magnetic minerals, and other rock-magnetic characteristics of sediments including composition, grain size, and interaction of magnetic minerals. If the sediments prove to be uniform rock-magnetically, variations of remanent intensity seen after normalizing the abundance of magnetic minerals using rock-magnetic parameters could be interpreted as relative changes of past geomagnetic-field strength (paleointensity). Because relative paleointensity variation during the last ~200 k.y. is relatively well understood (Yamazaki and Ioka, 1994; Guyodo and Valet, 1996), paleointensity can be used as a tool to correlate and estimate the age of sediments (paleointensity stratigraphy). If we assume that the relatively constant magnetic susceptibility of sediments from Sites 1078 and 1079 implies rock-magnetic homogeneity, ages of ~0.11 and ~0.19 Ma may be tentatively assigned to the remarkable lows in remanent intensity (labeled “A” and “B” in Fig-

ure 12) by comparison with the established magnetic paleointensity curve. This approach, however, must be thoroughly tested by post-cruise rock-magnetic studies.

### Magnetostratigraphy

Magnetic inclinations and declinations from all three holes indicate that only the Brunhes (C1n) normal polarity Chron (Berggren et al., 1995) is recorded in these sediments. An inclination of  $-23^\circ$  is expected from the geocentric axial dipole model (Fig. 11, middle and right panels). Whether the Brunhes is complete cannot be determined from the magnetostratigraphy.

Possible short reversal events and/or excursions in the Brunhes Chron, such as the Blake event, were not found at this site, in spite of the high sedimentation rate (~500 m/m.y.). Most anomalous directions seen in Figure 11 occur at boundaries of cores and/or sections and, thus, probably are caused by physical disturbance of the cores.

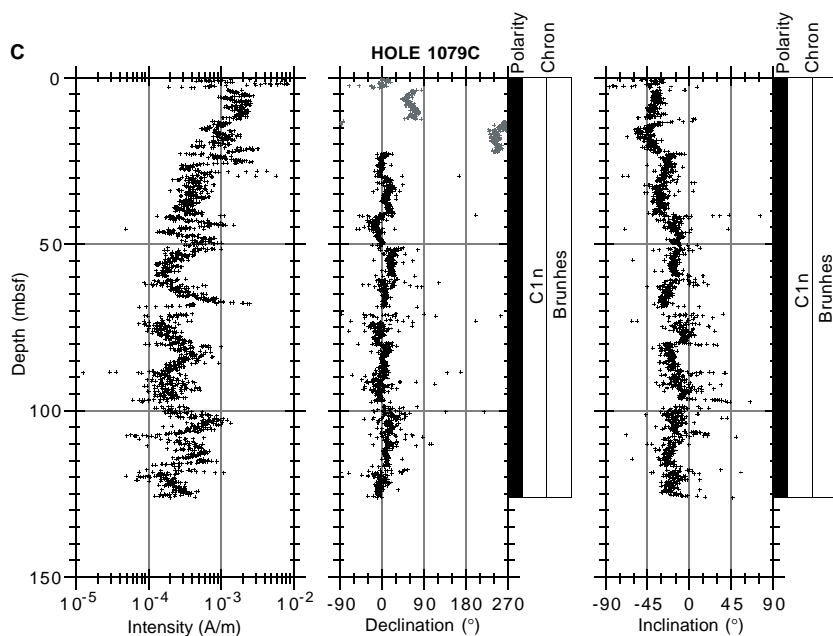


Figure 11 (continued). C. Hole 1079C.

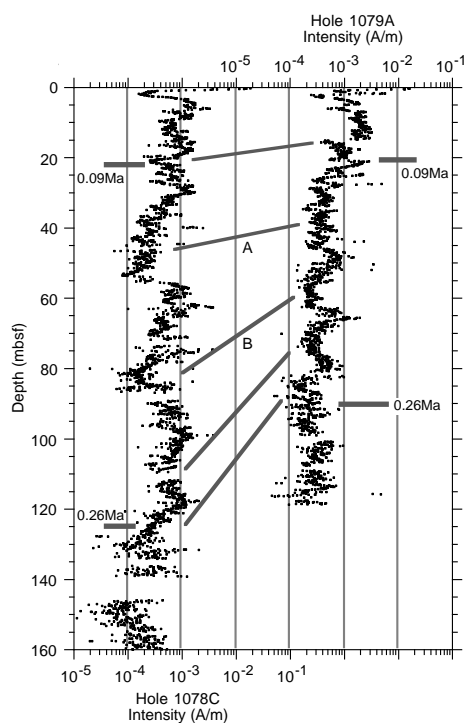


Figure 12. Possible correlation of sediments from Holes 1079A and 1078C using intensity of NRM. Two horizons with ages 0.09 and 0.26 Ma are based on nanofossil events. Intensity lows labeled “A” and “B” may correspond to paleointensity lows at  $\sim 0.11$  and  $\sim 0.19$  Ma, respectively (see text).

One possible cause for the absence of short reversal events is extensive bioturbation of sediments at this site. Many deep burrows, some of which continue vertically for more than 1 m, are present in the cores. This suggests that acquisition of postdepositional remanent magnetization (pDRM) occurs over a very wide zone (possibly more than 1 m) in shallow-water sediments, which reduces the resolution of past geomagnetic-field variations and filters out short reversal events. This contrasts with deep-sea sediments, where the lock-in

depth of pDRM is generally considered to occur within  $\sim 20$  cm (deMenocal et al., 1990), or possibly within a few centimeters below seafloor (Tauxe et al., 1996), and low sedimentation rates limit the resolution.

## COMPOSITE SECTION

At Site 1079, three holes were cored with the APC to a maximum depth of 129.9 meters below seafloor (mbsf). At the last sections of Holes 1079A and 1079B, as well as at several sections of Hole 1079C, flow-in structures were observed. These are described as pseudobedding parallel to the core liner and 1- to 2-cm-wide tubular structures penetrating the entire section (see “Lithostratigraphy” section, this chapter). Additional core disturbances caused by gas expansion are common at Site 1079.

The physical properties data set for Site 1079 included GRAPE density,  $P$ -wave velocity, and magnetic susceptibility, which were measured on the MST at 2-cm (Hole 1079A) and 4-cm intervals (Holes 1079B and 1079C). Natural gamma emissions were measured with a 32-cm sample interval on the MST. Color reflectance data were measured at 2-cm (Hole 1079A) and 4-cm intervals (Holes 1079B and 1079C). The correlation of features present in the physical and visual properties measurements of adjacent holes was used to demonstrate continuity of the stratigraphic sequence drilled and to establish a meters composite depth (mcd) scale for Site 1079. The continuity of the stratigraphic sequence was shown to 132 mcd.

At Site 1079, magnetic susceptibility and wet bulk density (GRAPE) were used to establish the mcd scale. The data sets were extensively processed before being used for correlation. Suspect measurements were eliminated by thresholding the data, followed by additional processing using a linear approximation filter algorithm. For 10 measurements, taken over an interval of 20 to 40 cm, a linear regression and the standard deviation of the data were calculated. Measurements with values outside twice the standard deviation were reassigned the linearly approximated value. Finally, the data were smoothed using a Gaussian filter with a length of 12 cm. All data shown in Figures 13 and 14 were processed as described above.

The stratigraphic correlation among Holes 1079A, 1079B, and 1079C is excellent up to  $\sim 75$  mcd. A core overlap of  $\sim 50\%$  at Hole 1079C compared with Holes 1079A and 1079B allowed for a good

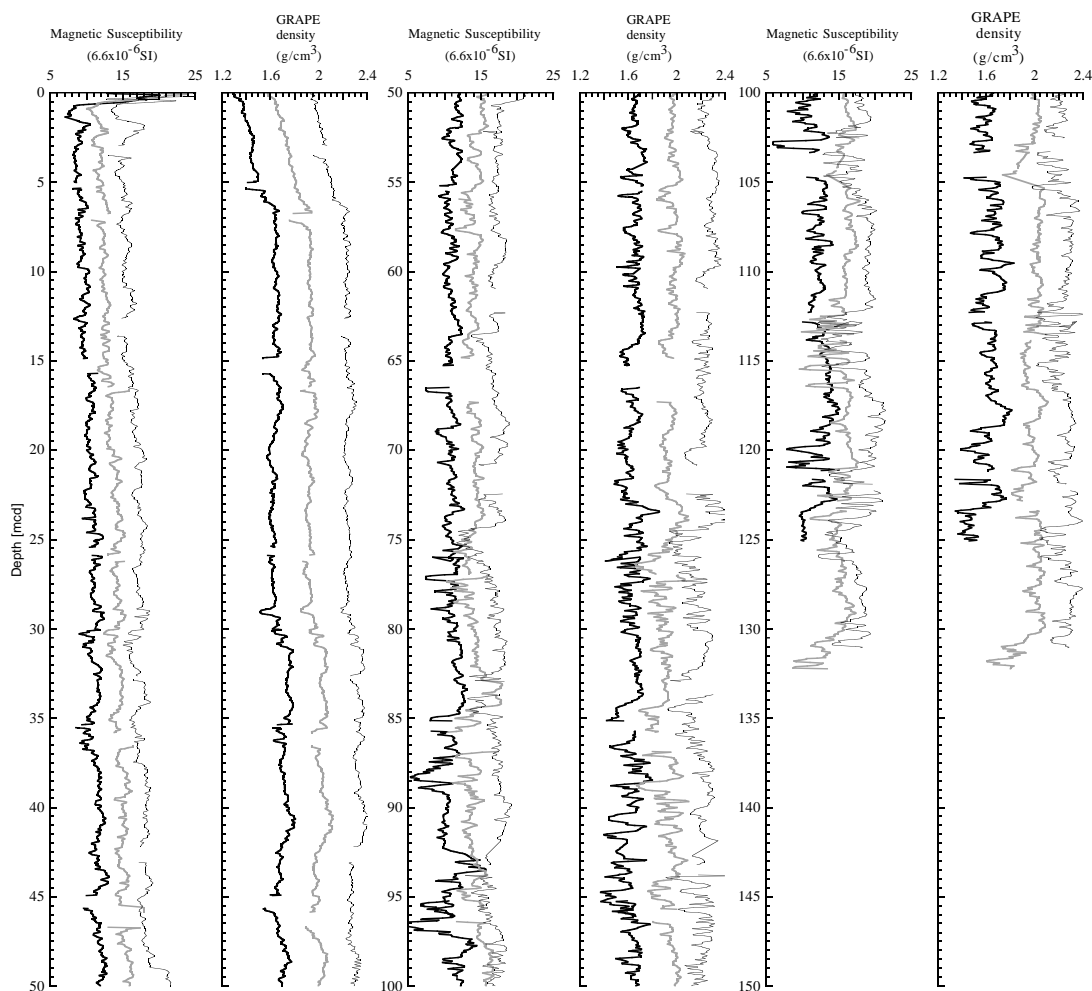


Figure 13. Composite section for Site 1079. Magnetic susceptibility and wet bulk density (GRAPE) are plotted for Holes 1079A (thin black line), 1079B (gray line), and 1079C (thick black line). Downhole logs are shown in meters composite depth (mcd). Offsets have been applied for clarity.

correlation of sedimentary features expressed in the magnetic susceptibility and wet bulk density logs. Below 75 mcd, coring disturbance and, possibly, gas expansion introduced a higher scatter in both data sets used. The magnetic susceptibility log appears to be intensively disturbed between 75 and 132 mcd. The interhole correlation of this parameter was very poor in this depth interval, and the logs show few features suitable for alignment. The GRAPE wet bulk density also exhibits some disturbance from 75 to 132 mcd. Major variations in the density record for Site 1079 are still distinguishable in this parameter. The alignment of these features demonstrates the completeness of the sedimentary sequence drilled at Site 1079 down to 132 mcd. The evaluation of color reflectance data, especially for the problematic interval from 75 to 132 mcd, revealed no additional information compared with GRAPE wet bulk density. The red/blue ratio (650/450 nm) shows a decreased amplitude compared with the Lower Congo Basin sites (see “Lithostratigraphy” section, this chapter, and the “Composite Section” and “Lithostratigraphy” sections in the “Site 1075,” “Site 1076,” and “Site 1077” chapters, this volume). The total reflectance data (lightness  $L^*$ ) of Site 1079 reveal more variation but are also affected by drilling disturbance (see “Lithostratigraphy” section, this chapter). According to the available data, an application of offsets to cores below ~80 mcd was not justified (Table 6; Fig. 15). Thus, compared with the standard ODP mbsf scale, the final growth of the mcd scale is less than 5% at Site 1079.

The spliced record presented in Figure 14 and Table 7 is continuous to 132 mcd for magnetic susceptibility and GRAPE wet bulk den-

sity. It was constructed using cores from Hole 1079A whenever possible. The spliced record could be constructed with very smooth transitions between the core fragments used in the upper half of Site 1079 (i.e., 0 to ~80 mcd; Fig. 14).

## INORGANIC GEOCHEMISTRY

Fifteen interstitial water samples were collected from Hole 1079A over a depth range from 1.4 to 120 mbsf (Table 8) at a typical frequency of one sample per core. On all profiles presented here, the chemical distributions at Site 1077, which are broadly representative of the sites drilled in the Congo Basin, and at Site 1078, the other Angola Basin site drilled during Leg 175, are provided for both inter- and intrabasin comparison purposes. At Site 1079, the dominant factor affecting the interstitial water chemical profiles is the low level of organic carbon preserved in the sediments (see “Organic Geochemistry” section, this chapter). Also, evidence suggests a brine influence near the base of the hole, as shown in the chemical profiles of dissolved sulfate,  $\text{Sr}^{2+}$ ,  $\text{Na}^+$ , and  $\text{K}^+$ , as well as of salinity.

### Alkalinity, Sulfate, and Ammonium

Downcore profiles of alkalinity, sulfate, and ammonium at Site 1079 (Fig. 16) are markedly different from those observed at the previous Leg 175 drill sites. Degradation of organic matter is the com-

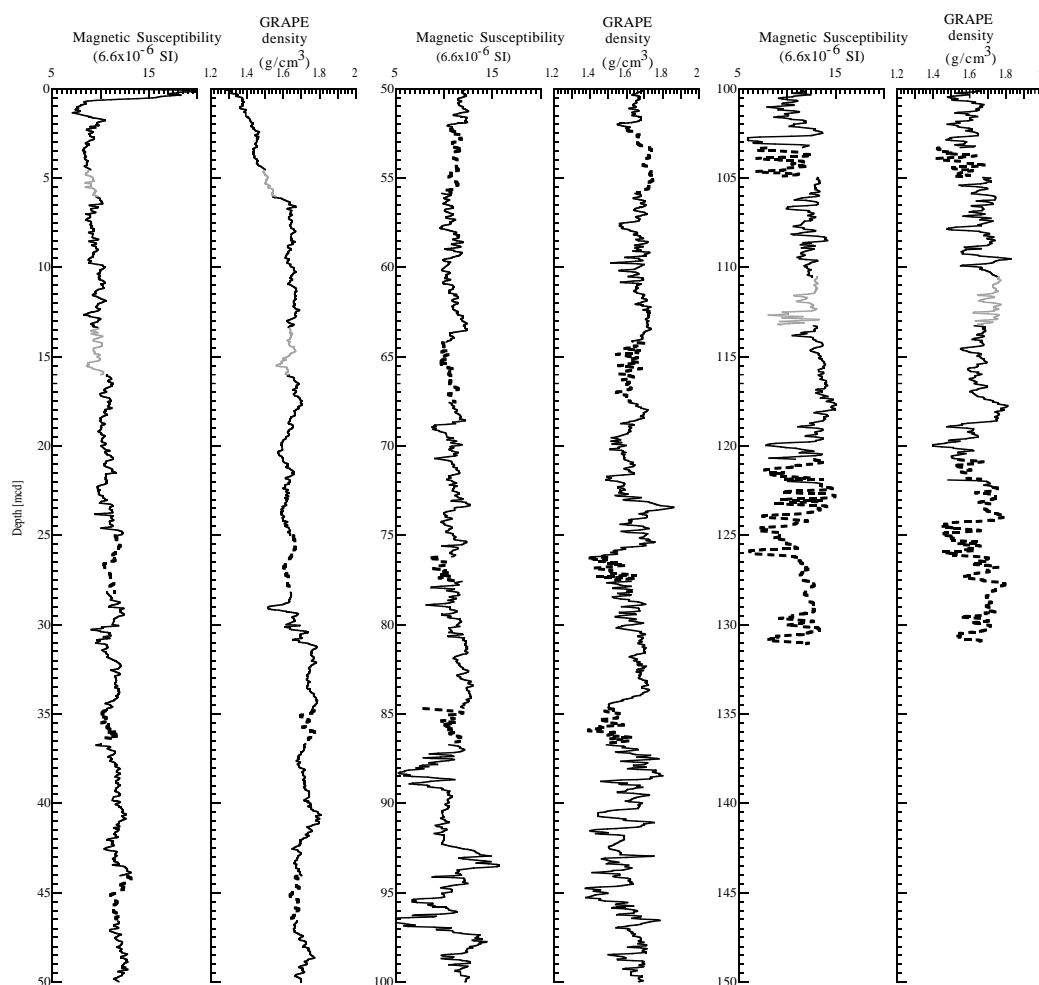


Figure 14. Spliced records for magnetic susceptibility and wet bulk density (GRAPE) plotted in meters composite depth (mcd). Cores from all three holes at Site 1079 have been used for the spliced record: solid black line = Hole 1079A, gray line = Hole 1079B, and dashed line = Hole 1079C.

mon process affecting alkalinity, ammonium, and sulfate at all the sites; at Site 1079 each of these components records relatively low rates of degradation. The alkalinity maximum is reached at ~110 mbsf, and the buildup of ammonium also is very slow, particularly in the upper portions of the section. Most significantly, the complete consumption of dissolved sulfate is achieved only at ~50 mbsf, which is the deepest stratigraphic position observed so far.

There are several possible causes for the contrast between these patterns and those observed at previous Leg 175 sites. The amount and/or nature of the organic matter can influence the rate of degradation of organic matter and hence the stratigraphic position of complete sulfate consumption; however, these aspects of the organic matter at Site 1079 are not significantly different from those at previous sites (see “Organic Geochemistry” section, this chapter). Sedimentation rate may also play an important role. In general, slow relative sedimentation rates allow the deeper diffusive resupply of sulfate from seawater, whereas in certain situations, relatively high sedimentation rates can act to preserve sulfate in interstitial waters provided the balance between sulfate addition by burial and sulfate depletion by organic degradation is in favor of the burial term. Because sedimentation rates at Site 1079 are, in fact, higher than those at all previous sites—except for Site 1078 (see “Biostratigraphy and Sedimentation Rates” section, this chapter)—we favor the latter option.

Concentrations of sulfate begin to increase in the deepest sections of the hole. As will be discussed later, this is evidence of a brine influence.

### Calcium, Magnesium, and Strontium

Within the uppermost 10 mbsf, concentrations of dissolved  $Mg^{2+}$ ,  $Ca^{2+}$ , and  $Sr^{2+}$  (Fig. 17) are essentially constant (or perhaps show a slight increase). From 10 to 48 mbsf, all three components decrease in concentration. A paired decrease of  $Mg^{2+}$  and  $Ca^{2+}$  in this interval is consistent with dolomite precipitation; however, the decrease in dissolved  $Sr^{2+}$  concentration suggests that perhaps the precipitation of fluorapatite may also be occurring, as we hypothesize for Site 1078. Below ~50 mbsf, the downcore profiles of  $Ca^{2+}$ ,  $Mg^{2+}$ , and  $Sr^{2+}$  exhibit a marked change. Concentrations of  $Ca^{2+}$  and  $Mg^{2+}$  remain essentially constant to the bottom of the hole, whereas the concentration of  $Sr^{2+}$  increases. Presumably, dissolution of biogenic carbonate is responsible for the increase of  $Sr^{2+}$ , and  $Ca^{2+}$  does not show a similar increase because of formation of authigenic carbonates, or apatite, or both.

### Silica and Phosphate

Dissolved silica increases in concentration very rapidly through the uppermost 4 mbsf of sediment (Fig. 18), recording the dissolution of biogenic silica. The concentration of silica continues to increase slightly at greater depths, but never reaches very high values. The concentrations of dissolved silica are closely similar to those at Site 1078 but are lower than those observed in the Congo Basin, reflecting

**Table 6. Offsets applied to cores from Holes 1079A, 1079B, and 1079C.**

Core	Depth (mbsf)	Offset (m)	Composite depth (mcd)
<b>175-1079A-</b>			
1H	0.0	0.00	0.00
2H	5.3	0.00	5.30
3H	14.8	0.86	15.66
4H	24.3	1.56	25.86
5H	33.8	1.68	35.48
6H	43.3	2.30	45.60
7H	52.8	2.68	55.48
8H	62.3	4.15	66.45
9H	71.8	4.15	75.95
10H	81.3	4.39	85.69
11H	90.8	4.39	95.19
12H	100.3	4.39	104.69
13H	108.4	4.39	112.79
14H	117.2	4.39	121.59
<b>175-1079B-</b>			
1H	0.0	0.00	0.00
2H	7.0	0.10	7.10
3H	16.5	0.10	16.60
4H	26.0	0.20	26.20
5H	35.5	1.04	36.54
6H	45.0	1.66	46.66
7H	54.5	1.42	55.92
8H	64.0	3.26	67.26
9H	73.5	3.46	76.96
10H	82.5	4.34	86.84
11H	92.0	4.34	96.34
12H	100.0	4.34	104.34
13H	109.5	4.34	113.84
14H	119.0	4.34	123.34
<b>175-1079C-</b>			
1H	0.0	0.00	0.00
2H	3.3	0.12	3.42
3H	12.8	0.76	13.56
4H	22.3	0.86	23.16
5H	31.8	1.00	32.80
6H	41.3	1.72	43.02
7H	50.8	1.30	52.10
8H	60.3	1.94	62.24
9H	69.8	2.60	72.40
10H	79.3	4.34	83.64
11H	88.8	4.94	93.74
12H	98.3	4.94	103.24
13H	107.8	4.94	112.74
14H	117.3	4.94	122.24

Note: The offsets transform ODP standard depth values in meters below seafloor (mbsf) to meters composite depth (mcd).

the lower concentration of diatoms at this site (see “Biostratigraphy and Sedimentation Rates” section, this chapter).

Dissolved phosphate increases to a maximum value of ~250 μM within the uppermost 40 mbsf. The maximum occurs at greater depth here at Site 1079 than at the previous sites, which is consistent with the lower amount of organic matter available for degradation and the greater depth of sulfate consumption discussed previously.

**Sodium and Potassium**

Concentrations of dissolved Na<sup>+</sup> steadily increase with depth downcore (Fig. 19), most likely reflecting cation exchange reactions involved with authigenic clay formation. Concentrations of dissolved K<sup>+</sup> reach a minimum value at ~50 mbsf before increasing to maximum values at the bottom of the hole. There are at least two potential mechanisms causing these increases. First, as observed at Site 1078, the paired behavior of these elements is different than that observed in the Congo Basin sites, suggesting that differences in clay mineralogy between the basins may exist. Alternatively, as mentioned below, the distributions of both these elements are also suggestive of a deep evaporite brine source.

**Brine Influence?**

There are several characteristic chemical distributions in the deep interstitial waters recovered from Site 1079 that are suggestive of the

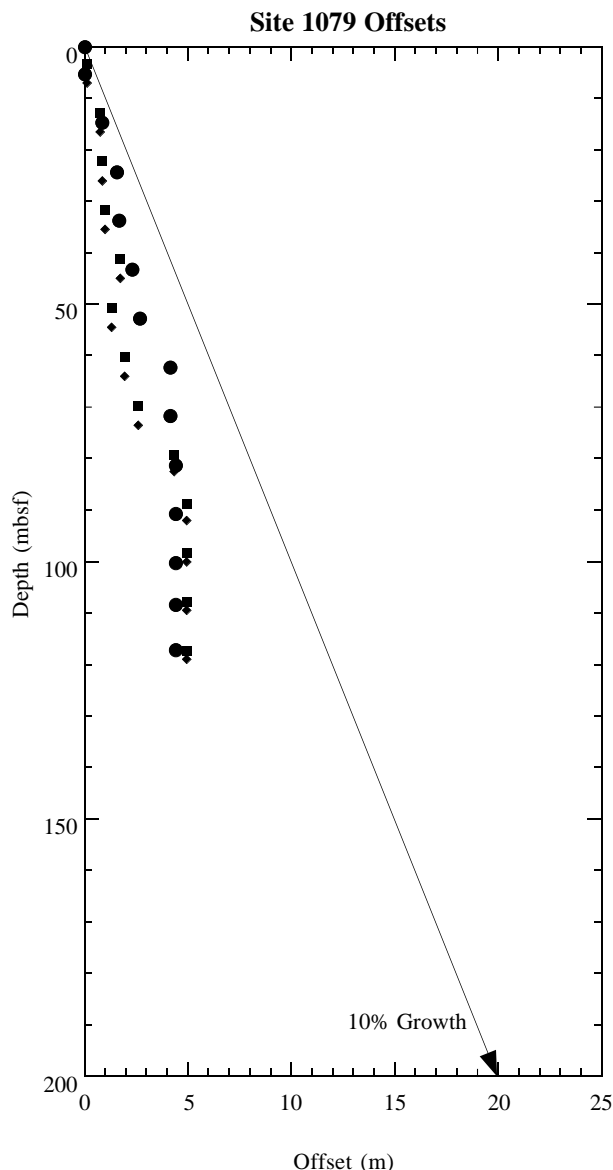


Figure 15. Offsets applied to Site 1079 cores plotted against standard ODP meters below seafloor (mbsf). A linear 10% growth of meters composite depth (mcd) compared with mbsf is indicated by an arrow. Offsets are plotted for Holes 1079A (circles), 1079B (diamonds), and 1079C (squares).

influence of evaporite dissolution and formation or migration of brine. As mentioned above, the concentration of sulfate begins to increase again starting at 80 to 100 mbsf, where values increase above zero and provide a maximum of 7 mM at the bottom of the hole (Table 8). This increase in sulfate is consistent with an evaporite source. Along with this increase in sulfate, salinity and dissolved Cl<sup>-</sup> also increase (Fig. 20). Other species also potentially sourced from a brine, including both Na<sup>+</sup> and K<sup>+</sup>, also increase. Although we cannot definitively state that these increases are caused by evaporite dissolution, the data (particularly the sulfate) appear consistent with such a source.

**ORGANIC GEOCHEMISTRY**

Calcium carbonate and organic carbon concentrations were measured on sediment samples from Hole 1079A (Table 9). Organic mat-

**Table 7. List of splice tie points used to create the continuous “spliced” stratigraphic sequence for Site 1079.**

Hole, core, section, interval (cm)	Depth (mbsf)	Composite depth (mcd)	Whether tied	Hole, core, section, interval (cm)	Depth (mbsf)	Composite depth (mcd)	Offset (m)
1079A-1H-4, 4	4.54	4.54	Tie to	1079B-1H-4, 4	4.54	4.54	0.00
1079B-1H-5, 4	6.04	6.04	Tie to	1079A-2H-1, 74	6.04	6.04	0.00
1079A-2H-6, 58	13.38	13.38	Tie to	1079B-2H-5, 28	13.28	13.38	0.10
1079B-2H-6, 140	15.90	16.00	Tie to	1079A-3H-1, 34	15.14	16.00	0.86
1079A-3H-7, 34	24.14	25.00	Tie to	1079C-4H-2, 33	24.14	25.00	0.86
1079C-4H-4, 52	27.32	28.18	Tie to	1079A-4H-2, 82	26.62	28.18	1.56
1079A-4H-7, 32	33.22	34.78	Tie to	1079C-5H-2, 48	33.78	34.78	1.00
1079C-5H-3, 84	35.64	36.64	Tie to	1079A-5H-1, 116	34.96	36.64	1.68
1079A-5H-6, 146	42.36	44.04	Tie to	1079C-6H-1, 101	42.32	44.04	1.72
1079C-6H-3, 56	44.86	46.58	Tie to	1079A-6H-1, 98	44.28	46.58	2.30
1079A-6H-5, 86	49.96	52.26	Tie to	1079C-7H-1, 16	50.96	52.26	1.30
1079C-7H-3, 76	54.56	55.86	Tie to	1079A-7H-1, 38	53.18	55.86	2.68
1079A-7H-6, 120	61.50	64.18	Tie to	1079C-8H-2, 44	62.24	64.18	1.94
1079C-8H-4, 80	65.60	67.54	Tie to	1079A-8H-1, 107.5	63.39	67.54	4.15
1079A-8H-7, 116	72.06	76.21	Tie to	1079C-9H-4, 10.5	73.61	76.21	2.60
1079C-9H-4, 144	74.94	77.54	Tie to	1079A-9H-2, 7.5	73.39	77.54	4.15
1079A-9H-6, 132	80.52	84.67	Tie to	1079C-10H-1, 102.5	80.33	84.67	4.34
1079C-10H-3, 4	82.34	86.68	Tie to	1079A-10H-2, 40	82.29	86.68	4.39
1079A-10H-8, 60	91.39	95.78	Tie to	1079A-11H-1, 58.5	91.39	95.78	4.39
1079A-11H-6, 72	98.92	103.31	Tie to	1079C-12H-1, 6.5	98.37	103.31	4.94
1079C-12H-2, 20	100.00	104.94	Tie to	1079A-12H-1, 23.5	100.55	104.94	4.39
1079A-12H-4, 144	106.14	110.53	Tie to	1079B-12H-5, 18.5	106.19	110.53	4.34
1079B-12H-6, 140	108.90	113.24	Tie to	1079A-13H-1, 43.5	108.85	113.24	4.39
1079A-13H-6, 56	116.36	120.75	Tie to	1079C-13H-6, 50.5	115.81	120.75	4.94
1079C-13H-7, 16	116.96	121.90	Tie to	1079A-14H-1, 30.5	117.51	121.90	4.39
1079A-14H-1, 72	117.92	122.31	Tie to	1079C-14H-1, 6.5	117.37	122.31	4.94
1079C-14H-6, 132	126.12	131.06					

Note: The tie points are listed in standard ODP meters below seafloor (mbsf) and meters composite depth (mcd).

**Table 8. Interstitial water composition for Hole 1079A.**

Core, section, interval (cm)	Depth (mbsf)	pH	Alkalinity (mM)	Salinity	Cl <sup>-</sup> (titr) (mM)	Cl <sup>-</sup> (IC) (mM)	SO <sub>4</sub> <sup>2-</sup> (mM)	Na <sup>+</sup> (mM)	Mg <sup>2+</sup> (mM)	Ca <sup>2+</sup> (mM)	K <sup>+</sup> (mM)	H <sub>4</sub> SiO <sub>4</sub> (μM)	NH <sub>4</sub> <sup>+</sup> (μM)	PO <sub>4</sub> <sup>3-</sup> (μM)	Sr <sup>2+</sup> (μM)
175-1079A-															
1H-1, 140-150	1.40	7.65	4.922	34.5	551	551	28.38	478	50.45	10.21	12.59	237	389	24	95
1H-3, 140-150	4.40	7.67	5.003	34.5	553	553	27.67	477	50.94	10.68	13.00	351	502	26	96
2H-2, 140-150	8.20	7.18	5.739	35.0	553	554	27.35	479	50.69	10.25	12.55	327	608	38	95
3H-3, 140-150	19.20	7.58	11.429	35.0	558	556	20.81	484	50.15	7.37	12.00	375	1,333	91	87
4H-3, 120-130	28.50	7.80	15.052	34.5	558	558	16.18	482	50.15	5.99	11.67	401	1,454	207	82
5H-3, 120-130	38.00	7.83	23.104	34.0	564	561	8.68	484	49.00	5.32	11.92	497	1,741	251	77
6H-3, 130-140	47.60	7.83	35.174	34.0	564	562	0.59	490	46.08	3.52	11.33	420	2,292	202	84
7H-3, 140-160	57.20	7.70	34.763	34.0	564	566	0.00	494	43.11	3.45	11.74	626	3,403	80	86
8H-2, 140-150	65.20	7.76	40.254	34.0	561	567	0.00	499	41.05	3.62	13.06	523	3,886	80	90
9H-2, 140-150	74.70	7.88	45.849	34.5	561	565	1.09	504	42.22	3.77	13.95	465	5,283	34	94
10H-4, 130-140	86.19	7.91		35.0	565	565	0.56		41.19	4.26	14.66	409	6,061	52	92
11H-3, 130-140	95.10	7.92	54.194	35.5	563	559	1.33	510	43.80	3.80	14.90	425	7,467	52	103
12H-3, 130-140	104.50	7.20	43.913	36.0	563	562	1.33	499	44.48	3.96	14.52	613	8,030	93	112
13H-3, 130-140	111.20	7.76	59.014	36.0	570	567	1.28	522	42.10	3.82	17.70	351	12,814	51	105
14H-3, 130-140	120.00	7.72	43.913	36.0	572	573	7.04	519	43.59	4.37	15.65	462	9,110	89	122

Notes: Cl<sup>-</sup> (titr) = analyzed by titration and Cl<sup>-</sup> (IC) = analyzed by ion chromatography. Empty cells = not analyzed.

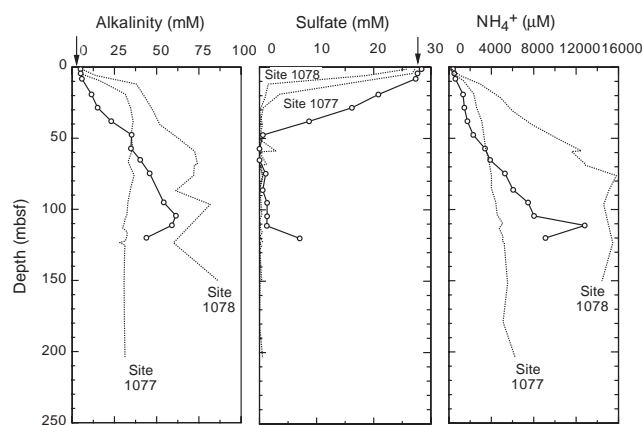


Figure 16. Downcore profiles of dissolved alkalinity, sulfate, and ammonium at Site 1079 (solid lines with open circles). Arrows = mean ocean-bottom-water values taken from Millero and Sohn (1992). For comparison, profiles for Site 1077 (Congo Basin) and Site 1078 (Angola Basin) are also shown (dotted lines).

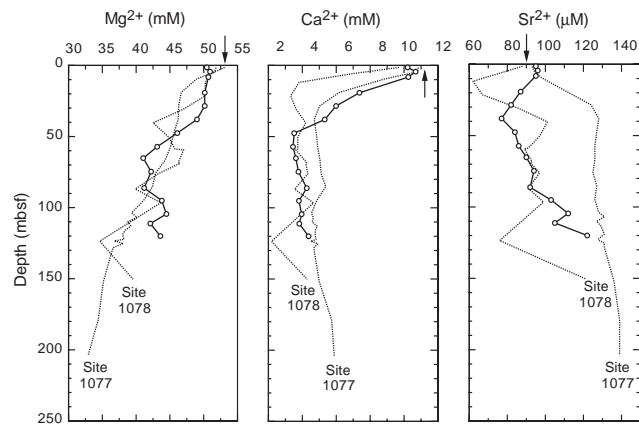


Figure 17. Downcore profiles of Ca<sup>2+</sup>, Mg<sup>2+</sup>, and Sr<sup>2+</sup> at Site 1079 (solid lines with open circles). Arrows = mean ocean-bottom-water values taken from Millero and Sohn (1992). For comparison, profiles for Site 1077 (Congo Basin) and Site 1078 (Angola Basin) are also shown (dotted lines).

ter atomic carbon/nitrogen (C/N) ratios and Rock-Eval pyrolysis analyses were employed to determine the type of organic matter contained within the sediments. High gas contents were encountered, and routine monitoring of the sedimentary gases was done for drilling safety.

### Inorganic and Organic Carbon Concentrations

Concentrations of carbonate carbon are rather low in Site 1079 sediments (Table 9). The maximum carbonate carbon concentration is equivalent to 17.9 wt% sedimentary CaCO<sub>3</sub>. These generally low concentrations agree with the paucity of coccoliths and foraminiferal microfossils in these hemipelagic sediments (see “Biostratigraphy and Sedimentation Rates” section, this chapter). The range in concentrations, although small, reflects a varying combination of changes in biological production of calcareous material, dilution by noncalcareous components, and carbonate dissolution fueled by oxidation of organic matter.

TOC determinations were done on a smaller number of Hole 1079A sediment samples than carbonate determinations because of the generally uniform lithology. TOC values range from 1.98 to 5.25 wt% (Table 9) and average 3.02 wt%. The concentrations are 10

times greater than the average of 0.3 wt% given by McIver (1975) based on Deep Sea Drilling Project (DSDP) Legs 1–33, a value that can be considered representative of typical deep-sea sediments. The high TOC concentrations at this site may be ascribed to a combination of elevated paleoproductivities and a high supply of organic matter from high accumulation rate of sediments, enhancing the preservation of organic matter.

### Organic Matter Source Characterization

Organic C/N ratios were calculated for Site 1079 samples using TOC and total nitrogen concentrations to help identify the origin of their organic matter. Site 1079 C/N ratios vary from 12.4 to 17.7 (Table 9). The C/N ratios average 15.3, which is a value that is intermediate between unaltered algal organic matter (5–8) and fresh land-plant material (25–35; e.g., Emerson and Hedges, 1988; Meyers, 1994). These organic carbon-rich sediments probably contain a mixture made up mostly of degraded algal material and partly of detrital continental organic matter. The C/N ratios that are higher than fresh algal organic matter indicate that preferential loss of nitrogen-rich, proteinaceous matter and consequent elevation of C/N ratios occurred during settling of organic matter to the seafloor. Such early diagenetic alteration of C/N ratios is often seen under areas of elevated marine productivity, such as the Angola margin (Meyers, 1997).

A Van Krevelen-type plot of the hydrogen index (HI) and oxygen index (OI) values (Table 10) suggests that the sediments contain a mixture of type II (algal) and type III (land-derived) organic matter (Fig. 21). Such an admixture of organic matter is consistent with the intermediate C/N ratios for these samples, which similarly suggest that the organic matter is constituted of marine and continental material. Another possibility—one that seems more likely—is that the sediments principally contain algal-derived organic matter that has been altered by microbial processing during early diagenesis. Well-preserved type II organic matter has high HI values (Peters, 1986), which can be lowered by microbial oxidation (Meyers, 1997). The low HI values of fresh type III organic matter, however, cannot become elevated by postdepositional alteration. In general, Hole 1079A sediments having lower Rock-Eval TOC values also have lower HI values (Fig. 22). This relationship confirms that the algal organic matter has been subject to much oxidation, which simultaneously lowers TOC and HI values. Further evidence of substantial amounts of in situ organic matter degradation exists in the large decreases in sulfate and increases in alkalinity in the interstitial waters of Site 1079 sediments (see “Inorganic Geochemistry” section, this chapter).

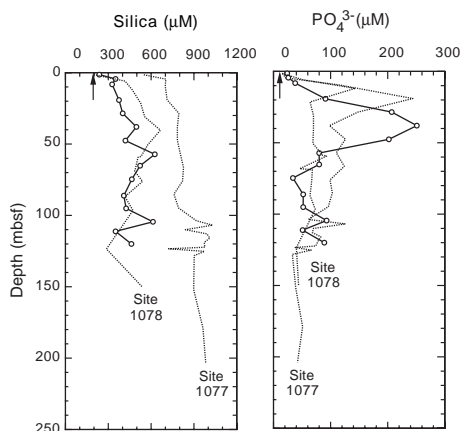


Figure 18. Downcore profiles of dissolved silica and phosphate at Site 1079 (solid lines with open circles). Arrows = mean ocean-bottom-water values taken from Millero and Sohn (1992). For comparison, profiles for Site 1077 (Congo Basin) and Site 1078 (Angola Basin) are also shown.

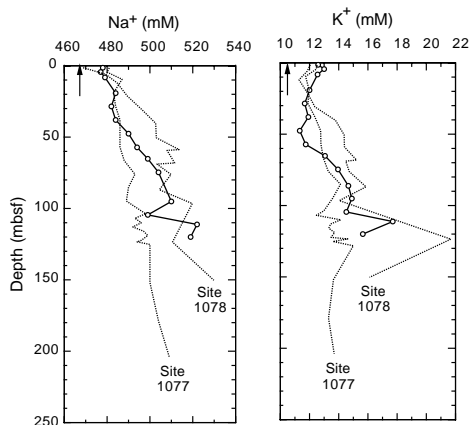


Figure 19. Downcore profiles of dissolved Na<sup>+</sup> and K<sup>+</sup> at Site 1079 (solid lines with open circles). Arrows = mean ocean-bottom-water values taken from Millero and Sohn (1992). For comparison, profiles for Site 1077 (Congo Basin) and Site 1078 (Angola Basin) are also shown (dotted lines).

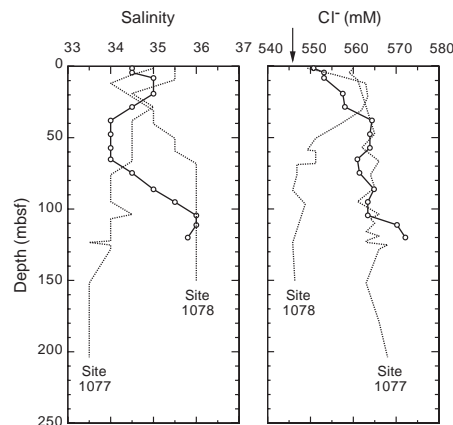


Figure 20. Downcore profiles of salinity and dissolved Cl<sup>-</sup> at Site 1079 (solid lines with open symbols). Arrow = mean ocean-bottom-water value taken from Millero and Sohn (1992). For comparison, profiles for Site 1077 (Congo Basin) and Site 1078 (Angola Basin) are also shown (dotted lines).

**Table 9. Percentages of inorganic and total carbon, total nitrogen, and total sulfur in sediment samples from Hole 1079A.**

Core, section, interval (cm)	Depth (mbsf)	IC (wt%)	CaCO <sub>3</sub> (wt%)	TC (wt%)	TOC (wt%)	TN (wt%)	TS (wt%)	C/N (atomic)
175-1079A-								
1H-1, 46-47	0.46	1.55	12.9	6.24	4.69	0.44	0.72	12.4
1H-3, 46-47	3.46	1.78	14.8	4.49	2.72	0.24	0.94	13.3
2H-1, 46-47	5.76	2.08	17.3	4.64	2.56	0.25	1.01	12.0
2H-3, 46-47	8.76	2.03	16.9					
2H-5, 46-47	11.76	1.92	16.0	4.38	2.46	0.22	1.03	13.1
3H-1, 46-47	15.26	1.78	14.9	4.60	2.82	0.20	1.26	16.3
3H-3, 46-47	18.26	1.78	14.8					
3H-5, 46-47	21.26	1.67	13.9	5.28	3.61	0.29	1.46	14.8
4H-1, 46-47	24.76	1.41	11.8	5.53	4.12	0.30	1.46	15.9
4H-3, 46-47	27.56	1.47	12.2					
4H-5, 46-47	30.36	2.02	16.8	4.58	2.56	0.18	1.15	17.1
5H-1, 46-47	34.26	2.32	19.3	4.40	2.08	0.17	1.09	14.3
5H-3, 46-47	37.26	1.84	15.3					
5H-5, 46-47	39.86	1.60	13.3	4.58	2.98	0.21	1.52	16.9
6H-1, 46-47	43.76	1.63	13.6	4.96	3.33	0.25	1.65	15.5
6H-3, 46-47	46.76	1.44	12.0					
6H-5, 46-47	49.56	1.35	11.2	4.75	3.40	0.25	2.08	15.7
7H-1, 46-47	53.26	1.66	13.8	4.74	3.09	0.22	1.48	16.4
7H-3, 46-47	56.26	2.15	17.9					
7H-5, 46-47	59.26	1.63	13.6	4.97	3.34	0.23	1.37	17.1
8H-1, 46-47	62.76	1.70	14.1					
8H-3, 46-47	65.76	0.83	6.9	6.07	5.25	0.37	2.20	16.7
8H-5, 46-47	68.36	2.01	16.8	4.93	2.92	0.23	1.72	15.0
9H-1, 46-47	72.26	1.86	15.5	4.53	2.67	0.19	1.53	16.3
9H-3, 46-47	75.26	2.14	17.8					
9H-5, 46-47	78.16	1.30	10.9	4.51	3.21	0.24	1.42	16.0
10H-1, 46-47	81.76	1.61	13.4	4.15	2.54	0.20	1.66	14.7
10H-3, 46-47	83.85	1.68	14.0					
10H-5, 46-47	86.75	1.54	12.9	3.53	1.98	0.13	1.21	17.7
11H-1, 46-47	91.26	1.03	8.6	4.44	3.41	0.24	1.85	16.7
11H-3, 46-47	94.26	1.16	9.7					
11H-5, 46-47	97.16	1.37	11.4	4.18	2.81	0.22	1.70	15.2
12H-1, 46-47	100.76	0.90	7.5	3.90	3.01	0.23	1.72	15.1
12H-3, 46-47	103.66	1.27	10.6					
12H-5, 46-47	106.66	1.50	12.5	3.82	2.32	0.17	1.25	16.0
13H-1, 46-47	108.86	1.35	11.2	3.67	2.32	0.19	1.46	14.3
13H-3, 46-47	111.86	1.04	8.7	3.88	2.84	0.22	1.73	15.1
13H-5, 46-47	114.76	1.63	13.6					
14H-1, 46-47	117.66	1.43	11.9	3.98	2.55	0.21	2.09	14.2

Notes: IC = inorganic carbon; CaCO<sub>3</sub> = calcium carbonate; TC = total carbon; TOC = total organic carbon; TN = total nitrogen; TS = total sulfur; and C/N = carbon/nitrogen ratio. TOC concentrations are calculated from the difference between IC and TC concentrations. C/N ratios are calculated from TOC and TN concentrations and are given as atom/atom ratios.

**Table 10. Results of Rock-Eval pyrolysis analyses of sediments from Hole 1079A.**

Core, section, interval (cm)	Depth (mbsf)	TOC (wt%)	S <sub>1</sub>	S <sub>2</sub>	S <sub>3</sub>	T <sub>max</sub> (°C)	HI	OI
175-1079A-								
1H-1, 46-47	0.46	4.69	2.99	8.86	5.82	407	370	124
2H-1, 46-47	5.76	2.56	0.61	17.39	4.13	412	253	161
4H-1, 46-47	24.76	4.12	0.95	6.48	4.02	415	275	97
5H-1, 46-47	34.26	2.08	0.48	11.37	2.84	414	208	136
6H-5, 46-47	49.56	3.40	0.73	4.34	3.60	418	217	105
8H-3, 46-47	65.76	5.25	2.21	7.38	4.26	408	375	81
10H-5, 46-47	86.75	1.98	0.29	19.72	2.55	414	170	128
12H-1, 46-47	100.76	3.01	0.68	3.38	3.12	416	240	103
14H-1, 46-47	117.66	2.55	0.35	7.23	2.71	422	209	106

Notes: TOC = total organic carbon; HI = hydrogen index; and OI = oxygen index. Units of the various Rock-Eval parameters are given in the "Organic Geochemistry" section of the "Explanatory Notes" chapter (this volume).

The sediment samples have relatively low Rock-Eval T<sub>max</sub> values, showing that their organic matter is thermally immature with respect to petroleum generation (Peters, 1986) and therefore contains little detrital organic matter derived from erosion of ancient sediments on the African continent.

### Headspace Gases

Sediments from Site 1079 had high gas content. Gas pressures became great enough in sediments below Core 175-1079A-4H (24 mbsf) to require perforating the core liner to relieve the pressure and prevent excessive core expansion. Natural gas analyses determined

that most of this gas was CO<sub>2</sub>, and headspace concentrations of this gas continued to increase to the bottom of Hole 1079A (120 mbsf; Fig. 23). Hydrogen sulfide could be detected by nose, but not by hydrogen sulfide-sensing instruments having a sensitivity of ~1 ppm, in Cores 175-1079A-1H through 8H (5–33.5 mbsf).

Methane (C<sub>1</sub>) first appears in headspace gas samples in Hole 1079A sediments at 28.6 mbsf. Concentrations gradually increase and become significant in sediments below 40 mbsf (Fig. 24). As at Sites 1075 through 1078, high methane/ethane (C<sub>1</sub>/C<sub>2</sub>) ratios and the absence of major contributions of higher molecular weight hydrocarbon gases (Table 11) indicate that the gas is biogenic, as opposed to thermogenic, in origin. A biogenic origin of the methane is supported by the disappearance of interstitial sulfate at approximately the same sub-bottom depth where methane concentrations begin to rise (see "Inorganic Geochemistry" section, this chapter). As noted by Claypool and Kvenvolden (1983), the presence of interstitial sulfate inhibits methanogenesis in marine sediments.

## PHYSICAL PROPERTIES

GRAPE density, magnetic susceptibility, and natural gamma radiation were measured near continuously with the MST on whole-round sections of cores from each hole (see "Explanatory Notes" chapter, this volume). Results from compressional (*P*-wave) ultrasonic velocity measurements with the MST were disregarded because of very high noise level.

Index properties (gravimetric density, porosity, and moisture content) were measured on one or two samples (volume = ~10 cm<sup>3</sup>) per

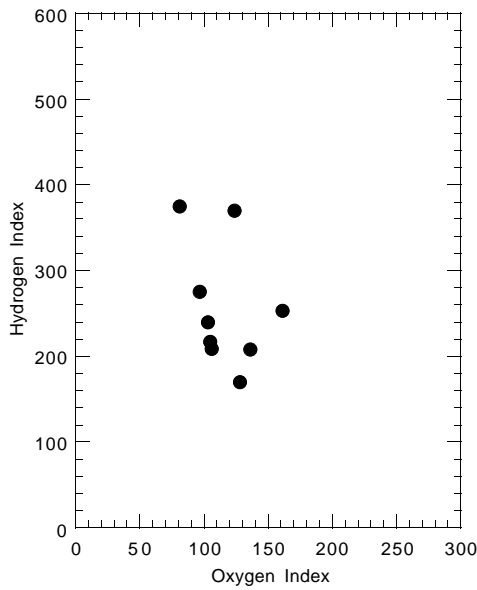


Figure 21. Rock-Eval Van Krevelen-type diagram of sediments from Hole 1079A. Organic matter appears to be a mixture of type II algal material that has been variably oxidized and type III continental or detrital organic matter. HI = milligrams of hydrocarbons per gram of organic carbon; OI = milligrams of CO<sub>2</sub> per gram of organic carbon.

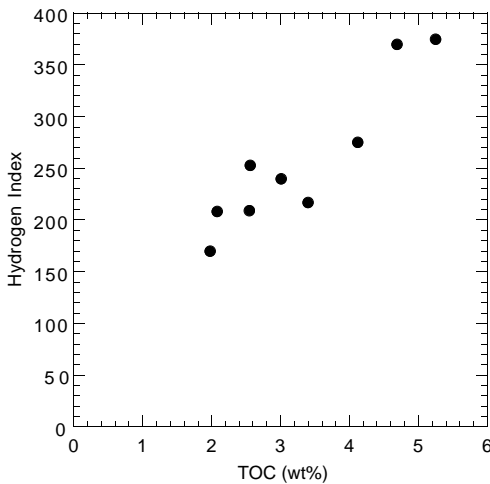


Figure 22. Comparison of Rock-Eval HI values and TOC concentrations of sediments from Hole 1079A. The correspondence between increases in both parameters indicates that preservation of marine organic matter is important to enhancing the organic carbon richness of sediments on the Angola margin.

working-half section on all cores from Hole 1079A, using Method C (see “Explanatory Notes” chapter, this volume).

Ultrasonic compressional (*P*-wave) velocities and undrained vane-shear measurements were conducted at a resolution of one or two samples per section near the index properties samples. The modified Hamilton Frame was used for the discrete *P*-wave measurements.

### Multisensor Track

The sampling interval for GRAPE density (Fig. 25A–C) and magnetic susceptibility measurements (Fig. 26A) was 2 cm for the upper

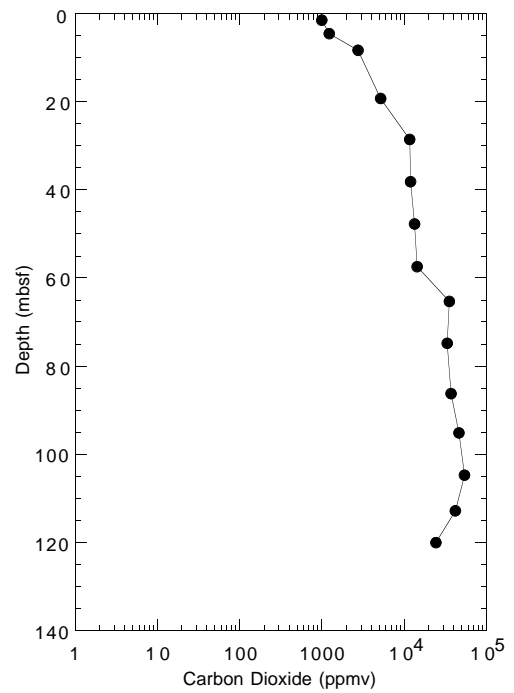


Figure 23. Headspace CO<sub>2</sub> concentrations in sediments from Hole 1079A.

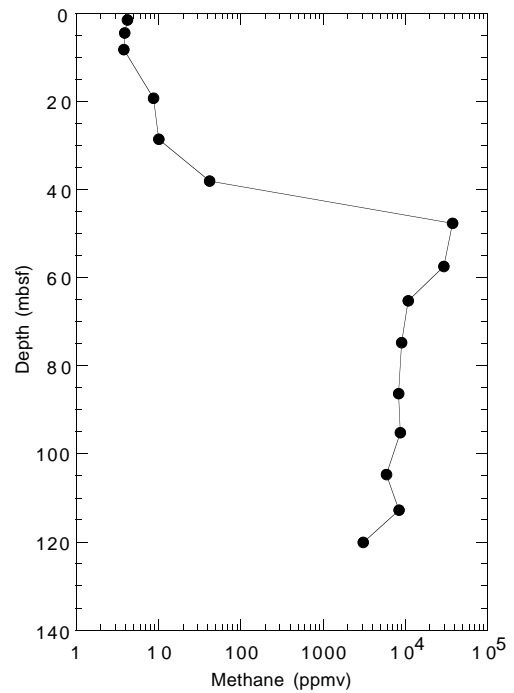


Figure 24. Headspace methane concentrations in sediments from Hole 1079A.

60 (mbsf and 4 cm below 60 mbsf. MST data are included on CD-ROM (back pocket, this volume). Natural gamma radiation was measured with a sampling period of 30 s at 32-cm resolution (Fig. 26B). Magnetic susceptibility and natural gamma radiation show some similarities in their profiles (Fig. 26A and B, respectively), but seem to reveal a phase difference. GRAPE density matches well with the discrete wet bulk density data (Fig. 25).

## Velocities

The near-continuous velocity profile recorded with the MST was disregarded because of instrumental problems and high scatter caused by degassing and voids. Discrete velocities range between 1510 and 1655 m/s (Fig. 27) with an increase around 5 mbsf and a steep increase at 28 mbsf. The same characteristics are observed in the density measurements (see below) and may be related to higher carbonate content in the silty clay-rich sediments (see “Lithostratigraphy” and “Inorganic Geochemistry” sections, this chapter). High-quality discrete ultrasonic signals were recorded between 0 and 52 mbsf and show an abrupt, complete attenuation below 52 mbsf.

## Index Properties

Results of discrete measurements of wet bulk density, porosity, and moisture content are presented in Figures 28A, 28B, and 28C, respectively (also see Table 12 on CD-ROM, back pocket, this volume). The density values vary between 1300 and 1960 kg/m<sup>3</sup>, and show higher values in intervals of higher carbonate content (see “Lithostratigraphy” section, this chapter). A varying proportion of abundant clay minerals and bigger grain sizes may be indicated by the porosity profiles, which shows a decrease from 85% in the top section to values as low as 49% at 120 mbsf. Discrete density values are lower than GRAPE values between 0 and 52 mbsf (Fig. 25A) and are higher below that depth (Fig. 25B, C). The shape of both profiles is very similar, revealing good coherence between the two measurements. A good correlation between the velocity and wet bulk density profiles can be observed between 0 and 52 mbsf.

## Thermal Conductivity

The thermal conductivity profile at Hole 1079A was measured by inserting a single probe into every second core section (see “Explanatory Notes” chapter, this volume). The values show significant scatter over the entire depth range, with an overall tendency to lower values below 40 mbsf (Fig. 26C).

**Table 11. Results of headspace gas analyses of sediments from Hole 1079A.**

Core, section, interval (cm)	Depth (mbsf)	C <sub>1</sub> (ppmv)	CO <sub>2</sub> (ppmv)	C <sub>2</sub> = (ppmv)	C <sub>2</sub> (ppmv)	C <sub>3</sub> (ppmv)	C <sub>1</sub> /C <sub>2</sub>
175-1079A-							
1H-2, 0-5	1.50	4.2	1,002				
1H-4, 0-5	4.50	3.9	1,230	0.1			
2H-3, 0-5	8.30	3.8	2,741				
3H-4, 0-5	19.30	8.7	5,148				
4H-4, 0-5	28.60	10.1	11,672		0.2		50
5H-4, 0-5	38.10	41.8	12,002		0.7		60
6H-4, 0-5	47.70	37,736	13,402	0.1	8.9	0.5	4,240
7H-4, 0-5	57.40	29,589	14,375	0.2	9.8	1.3	3,019
8H-3, 0-5	65.30	10,851	35,672		9.8	1.8	1,107
9H-3, 0-5	74.80	9,080	33,264	0.1	6.8	1.5	1,335
10H-5, 0-5	86.29	8,280	37,144	0.1	6.9	2.2	1,200
11H-4, 0-5	95.20	8,658	46,628	0.1	12.0	3.4	722
12H-4, 0-5	104.70	5,854	54,410	0.1	6.0	1.7	976
13H-4, 0-5	112.80	8,391	42,124	0.1	4.7	1.2	1,785
14H-3, 0-5	120.10	3,101	24,281	0.1	2.8	0.8	1,108

Notes: C<sub>1</sub> = methane; CO<sub>2</sub> = carbon dioxide; C<sub>2</sub>= = ethene; C<sub>2</sub> = ethane; and C<sub>3</sub> = propane. Dominance of C<sub>1</sub> over C<sub>2</sub> indicates that the gases originate from in situ microbial degradation of organic matter.

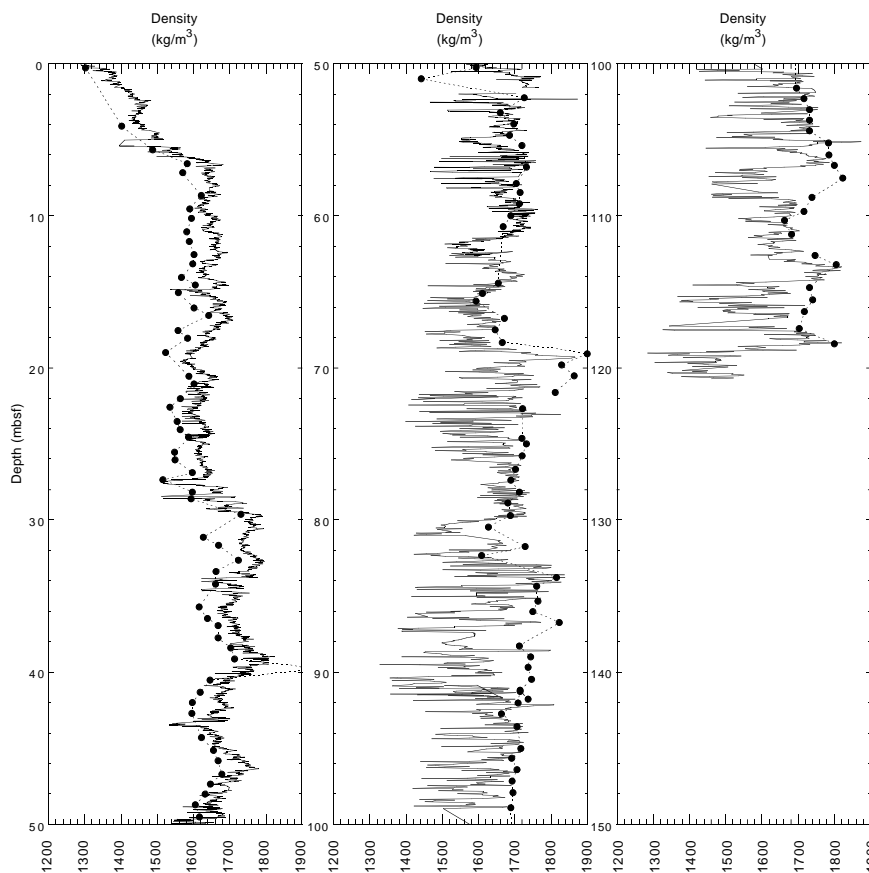


Figure 25. Discrete wet bulk density values (solid circles) compared with the GRAPE density profile (solid line) at Hole 1079A.

## Vane Shear Strength

An undrained vane-shear measurement was performed in the bottom part of each core section. The profile shows a gradual increase of shear-strength values from the top to 110 mbsf (Fig. 26D). The observed shape of vane-shear curves within each core may be related to the differential pressure within the core liners and variable sediment distortion. Consequently, lower shear-strength values were often measured close to the top and bottom of each core. The downhole trend among maximum values in each core correlates well with the wet bulk density measurements and reflects increasing compaction.

## REFERENCES

- Bé, A.W.H., and Tolderlund, D.S., 1971. Distribution and ecology of living planktonic foraminifera in surface waters of the Atlantic and Indian Oceans. In Funnel, B.M., and Riedel, W.R. (Eds.), *The Micropaleontology of Oceans*: Cambridge (Cambridge Univ. Press), 105–149.
- Berggren, W.A., Kent, D.V., Swisher, C.C., III, and Aubry, M.-P., 1995. A revised Cenozoic geochronology and chronostratigraphy. In Berggren, W.A., Kent, D.V., Aubry, M.-P., and Hardenbol, J. (Eds.), *Geochronology, Time Scales and Global Stratigraphic Correlation*. Spec. Publ.—Soc. Econ. Paleontol. Mineral. (Soc. Sediment. Geol.), 54:129–212.
- Claypool, G.E., and Kvenvolden, K.A., 1983. Methane and other hydrocarbon gases in marine sediment. *Annu. Rev. Earth Planet. Sci.*, 11:299–327.
- deMenocal, P.B., Ruddiman, W.F., and Kent, D.V., 1990. Depth of post-depositional remanence acquisition in deep-sea sediments: a case study of the Brunhes-Matuyama reversal and oxygen isotopic Stage 19.1. *Earth Planet. Sci. Lett.*, 99:1–13.
- Emerson, S., and Hedges, J.I., 1988. Processes controlling the organic carbon content of open ocean sediments. *Paleoceanography*, 3:621–634.
- Guyodo, Y., and Valet, J.-P., 1996. Relative variations in geomagnetic intensity from sedimentary records: the past 200,000 years. *Earth. Planet. Sci. Lett.*, 143:23–36.
- Imbrie, J., Hays, J.D., Martinson, D.G., McIntyre, A., Mix, A.C., Morley, J.J., Pisias, N.G., Prell, W.L., and Shackleton, N.J., 1984. The orbital theory of Pleistocene climate: support from a revised chronology of the marine  $\delta^{18}\text{O}$  record. In Berger, A., Imbrie, J., Hays, J., Kukla, G., and Saltzman, B. (Eds.), *Milankovitch and Climate* (Pt. 1), NATO ASI Ser. C, Math Phys. Sci., 126:269–305.
- Martini, E., 1971. Standard Tertiary and Quaternary calcareous nannoplankton zonation. In Farinacci, A. (Ed.), *Proc. 2nd Int. Conf. Planktonic Microfossils Roma*: Rome (Ed. Tecnosci.), 2:739–785.
- McIver, R.D., 1975. Hydrocarbon occurrences from JOIDES Deep Sea Drilling Project. *Proc. Ninth Petrol. Congr.*, 269–280.
- Meyers, P.A., 1994. Preservation of elemental and isotopic source identification of sedimentary organic matter. *Chem. Geol.*, 144:289–302.
- , 1997. Organic geochemical proxies of paleoceanographic, paleolimnologic, and paleoclimatic processes. *Org. Geochem.*, 27:213–250.
- Millero, F.J., and Sohn, M.L., 1992. *Chemical Oceanography*: Boca Raton (CRC Press).
- Okada, H., and Bukry, D., 1980. Supplementary modification and introduction of code numbers to the low-latitude coccolith biostratigraphic zonation (Bukry, 1973; 1975). *Mar. Micropaleontol.*, 5:321–325.
- Peters, K.E., 1986. Guidelines for evaluating petroleum source rock using programmed pyrolysis. *AAPG Bull.*, 70:318–329.
- Tauxe, L., Herbert, T., Shackleton, N.J., Kok, Y.S., 1996. Astronomical calibration of the Matuyama-Brunhes boundary: consequences for magnetic remanence acquisition in marine carbonates and the Asian loess sequences. *Earth Planet. Sci. Lett.*, 140:133–146.
- van der Gaast, S.J., and Jansen, J.H.F., 1984. Mineralogy, opal, and manganese of Middle and Late Quaternary sediments of the Zaire (Congo) deep-sea fan: origin and climatic variation. *Neth. J. Sea Res.*, 17:313–341.
- Weaver, P.P.E., 1993. High resolution stratigraphy of marine Quaternary sequences. In Hailwood, E.A., and Kidd, R.B. (Eds.), *High Resolution Stratigraphy*. Geol. Soc. Spec. Publ. London, 70:137–153.
- Yamazaki, T., and Ioka, N., 1994. Long-term secular variation of the geomagnetic field during the last 200 kyr recorded in sediment cores from the western equatorial Pacific. *Earth Planet. Sci. Lett.*, 128:527–544.

Ms 1751R-107

**NOTE: Core-description forms (“barrel sheets”) and core photographs can be found in Section 4, beginning on page 581. Forms containing smear-slide data can be found on CD-ROM. See Table of Contents for materials contained on CD-ROM.**

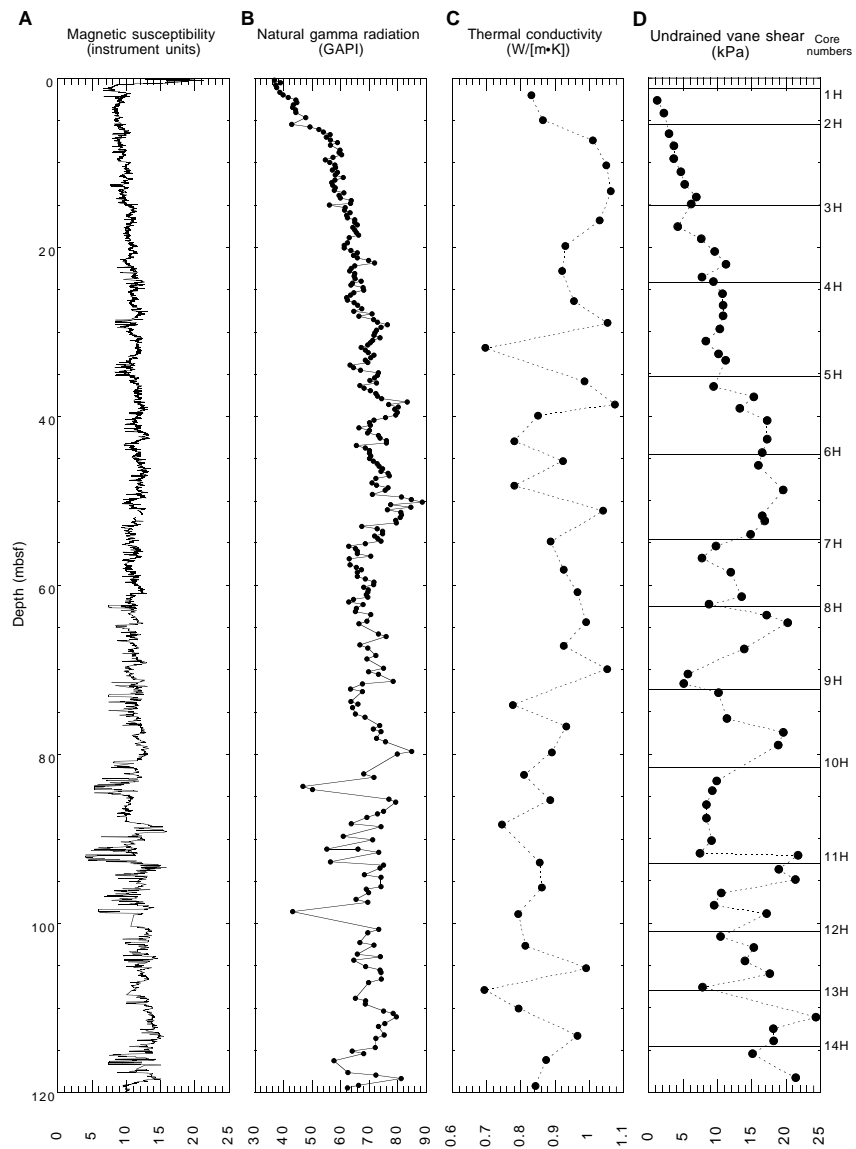


Figure 26. Plots of (A) magnetic susceptibility and (B) natural gamma radiation from MST measurements compared with discrete values of (C) thermal conductivity and (D) undrained vane shear strength at Hole 1079A.

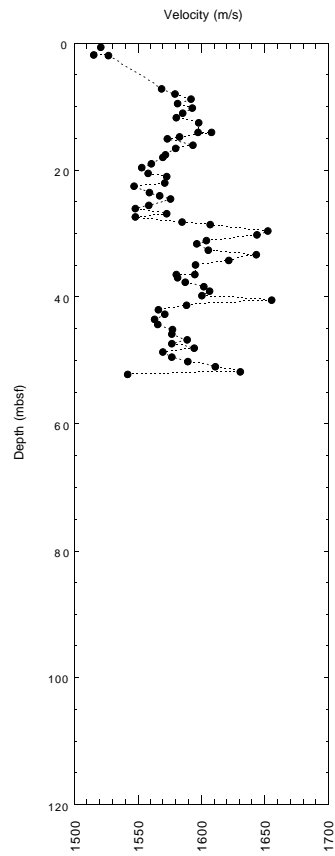


Figure 27. Discrete velocity profile measured at Hole 1079A.

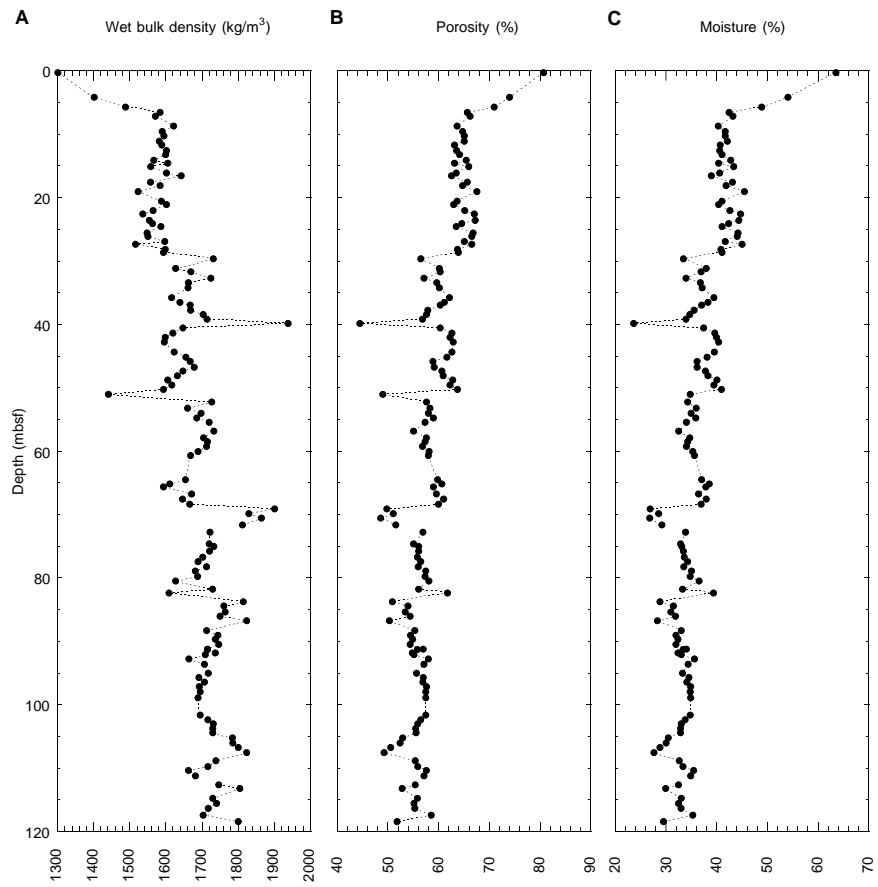


Figure 28. Plots of (A) wet bulk density, (B) porosity, and (C) moisture content derived from index properties measurements for Hole 1079A.